Helsinki University of Technology Control Engineering Laboratory

Espoo 2006 Report 147

MICROGRID MODELLING AND SIMULATION

Faisal Mohamed

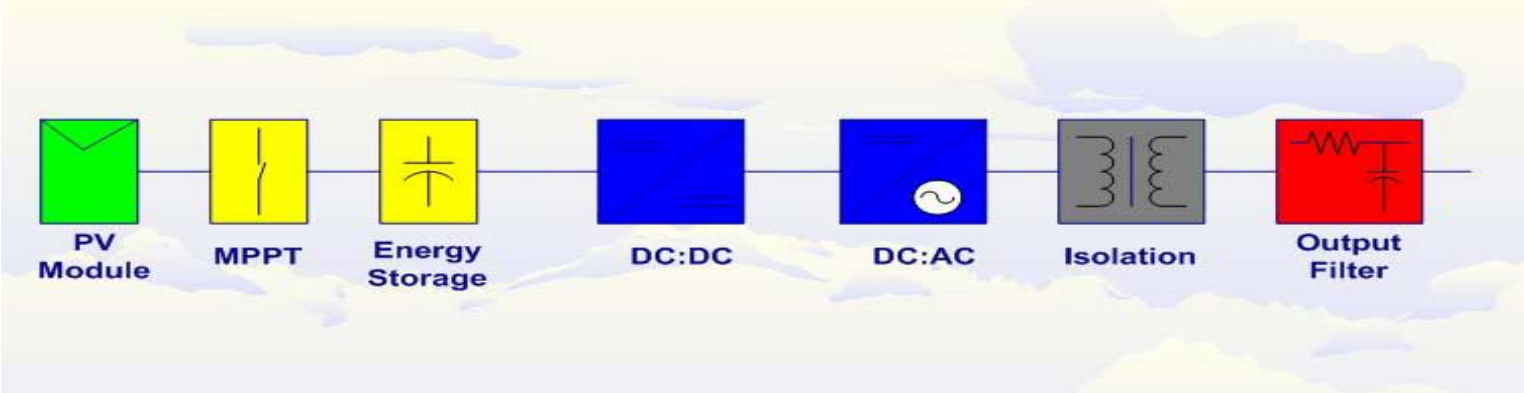

TEKNILLINEN KORKEAKOULU
TEKNISKA HÖGSKOLAN
HELSINKI UNIVERSITY OF TECHNOLOGY
TECHNISCHE UNIVERSITÄT HELSINKI
UNIVERSITE DE TECHNOLOGIE D´HELSINKI

Helsinki University of Technology Control Engineering Laboratory

Espoo March 2006 Report 147

MICROGRID MODELLING AND SIMULATION[1]

Faisal Mohamed

Abstract: A new concept in power generation is a microgrid. The Microgrid concept assumes a cluster of loads and microsources operating as a single controllable system that provides both power and heat to its local area. Not much is known about Microgrid behavior as a whole system. Some models exist which describe the components of a Microgrid. This thesis aims to model Microgrids at steady state and study their transient responses to changing inputs. Currently models of a Diesel Engine, a Fuel Cell, a Microturbine, a Wind turbine, and finally a Photovoltaic cell have been developed. It is intended that the work completed in this thesis will lay the groundwork for further model development. The long term goal is to have a highly sophisticated, complete system model of a Microgrid, so as to allow its simulation to fully understand how microgrids behave. The goal of this thesis is to build a complete model of Microgrid including the power sources, their power electronics, and a load and mains model in MATLAB/Simulink.

Keywords: microgrid, diesel engine, fuel cell, microturbine, wind turbine, photovoltaic, genetic algorithms

Helsinki University of Technology
Department of Automation and Systems Technology
Control Engineering Laboratory

[1] Thesis for the degree of Licentiate of Science in Technology, March 2006.

Distribution:
Helsinki University of Technology
Control Engineering Laboratory
P.O. Box 5500
FIN-02015 HUT, Finland
Tel. +358-9-451 5201
Fax. +358-9-451 5208
E-mail: control.engineering@hut.fi
http://www.control.hut.fi/

ISBN-13 978-951-22-8417-7
ISBN-10 951-22-8417-0
ISSN 0356-0872

Picaset Oy
Helsinki 2006

Acknowledgements

I joined Helsinki University of Technology, Control Engineering Laboratory as postgraduate student in July 2003.

First of all I would like to thank Allah for blessing me with ability to complete this work. This work couldn't be complete without help and support of several people.

First my deep gratitude goes to my advisor, Professor Heikki Koivo who has provided invaluable support, guidance, patience, and encouragement over the past years. I would like to thank all my Libyan friends here in Helsinki, and in Libya for their care and encouragement. I wish also to thank all the my friends and colleagues in the Control Engineering Laboratory, for creating a friendly and stimulating atmosphere.

My deep appreciation are for all my family and relatives at home, for their support and encouragement. Also I thank my wife and my children for their patience, ultimate support, great generosity, and lovingness.

This thesis has been supported by grant from Omar Al-Mukhtar University- El-Beida - Libya.

Thanks to everyone who has contributed to this work by anyhow directly or indirectly.

Otaniemi, March 20, 2006

FAISAL MOHAMED

Contents

Abbreviations And List of Symbols

1. ABBREVIATIONS

AFC	Alkaline Fuel Cell
CHP	Combined Heat and Power
CI	Compression Ignition
DG	Distributed Generation
FC	Fuel cell
GA	Genetic Algorithms
IGBT	Insulated Gate Bipolar Transistor
IGBT	Insulated Gate Bipolar Transistor
MCFC	Molten Carbonate Fuel Cell
MG	MicroGrid
MPPT	Maximum Power Point Tracking
MT	Micro Turbine
NOCT	Normal Operating Cell Temperature
PAFC	Phosphoric Acid Fuel Cell
PCC	Point of Common Coupling
PEMFC	Proton Exchange Membrane Fuel Cell
PI	Proportional, Integral
PID	Proportional, Integral, Derivative
PMSG	Permanent Magnet Synchronous Generator
PRBS	Pseudo Random Binary Signal
PV	Photovoltaic
PWM	Pulse Width Modulation
RLS	Recursive Least Squares
SD	Separation Device
SI	Spark Ignition
SOFC	Solid Oxide Fuel Cell
UPS	Uninterruptible Power Supply

2. SYMBOLS

$\xi(t)$	Uncorrelated Zero Main Random Sequence
N_i^r	Reaction Rate of the ith Reactant
δ_e	Grid Voltage Phase Angle
δ_V	Inverter Terminal Voltage Phase Angel
δ_P	Power Angle
γ	Forgetting Factor
ω_0	Input to the P Setpoint Block
ω_e	Grid Frequency
ω_m	Mechanical Frequency of the Generator
ω_s	Stator Electrical Frequency
ω_w	Angular Speed of a Flywheel
ω	Electrical Angular Frequency
ψ	flux Linkage
$\Phi(s)$	Fuel-Flow
ρ	Viscous Friction Coefficient
$\tau_{1\,\max}$	Upper Limit Values of the Dead Time
$\tau_{1\,\min}$	Lower Limit Values of the Dead Time
τ_{H_2}	Time Constant of the System Associated with the Hydrogen Flow
τ_1	Time Delay
τ_2	Actuator Time Constant
θ^T	Parameter Vector
$\varphi^T(t)$	Data Vector
ϑ	Density of Air
A_{cf}	Curve Fitting Constant
C_p	Power Coefficient
$e(t)$	Control Error Signal
E_{ac}	System Voltage
E_{GO}	Band Gap for Silicon
E_0	Voltage associated with the Reaction Free Energy
E_g	No Load DC Voltage
F	Faraday's Constant
g_i	Factor of Adaptive Sensitivity
G	Solar Irradiation

H_m	Equivalent Inertia Constant of the Generator Rotor
i	Current
$I(s)$	Input Current For the Diesel Engine
I^r	Stack Current
I_{or}	Cell Saturation Current
I_{os}	Cell Reverse Saturation Current
I_{sh}	Shunt-Leakage Current
I_{SCR}	Short Circuit Current
I_D	Diode-Current
$J(s^{-1})$	Plant and Flywheel Acceleration
k_c	Proportional Gain
K	Valve Constant
K_{an}	Anode Valve Constant
K_B	Boltzmann Constant
K_{H_2}	Valve Molar Constant for Hydrogen
K_{H_2O}	Valve Molar Constant for Water
K_0	Process Gain
K_1	Engine Torque Constant
K_2	Fuel Actuator Gain
K_3	Actuator and the Current Driver Constant
K_I	Short Circuit Current Temperature Coefficient
K_r	Constant Defined for Modelling Purposes
K_v	Voltage Constant
L_m	Mutual Inductance
L_r	Rotor Leakage Inductances
L_s	Stator Leakage Inductances
n_{H_2}	Number of Hydrogen Moles in the Anode Channel
N_0	Number of Cells Associated in Series in the Stack
N_i^{in}	Flow Rates Reactant at the Cell Input
N_i^0	Flow Rates Reactant at the Cell Output
P	Active Power
P^*	Output Power from the Control Unit
P_{H_2O}	Partial Pressure of Water
P_{H_2}	Partial Pressure of Hydrogen
P_{min}	Minimum Power Point
P_{mpp}	Maximum Power Point
P_m	Input Power
P_ru	Pressure Upstream

q	Electron Charge
q_{H_2}	Molar flows of Hydrogen
$q_{H_2}^{in}$	Input Hydrogen Molar Flow
$q_{H_2}^{out}$	Output Hydrogen Molar Flow
$q_{H_2}^{r}$	Hydrogen Molar Flow Take Part in the Reaction
q_{H_2O}	Molar flows of Water
Q	Reactive Power
r	Reference Signal
R	Resistance
R_s	Series Resistance
R_{sh}	Shunt Resistance
s	rotor slip
t	Time
T	Cell Temperature
$T(s)$	Mechanical torque of Diesel Engine
T_D	Derivative Time
T_I	Integral Time
T_m	Mechanical Shaft Torque for the no Loss System
T_r	Reference Temperature
T_t	Load Torque
$u(t)$	System Input
U	Terminal Voltage of the PV cell
$U_{\max}$	Maximum Fuel Utilization
$U_{\min}$	Minimum Fuel Utilization
U_{oc}	Open Circuit Voltage
U_{opt}	Optimal Fuel Utilization
U_f	Fuel Utilization
v	Voltage
V	Cell Volume
V_w	Wind Velocity
V^*	Output Voltage from the Control Unit
V_{ac}	AC Voltage
V_{dc}	DC Voltage
V_{LL}	Voltage Induced on the Generator Terminal
V_{mpp}	Voltage at Maximum Power Point
Vo	Cell Volume

W	Mass Flow
W_{an}	Mass Flow Through the Anode Valve
X_L	Reactance
$y(t)$	System Output
z^{-1}	Backward Shift Operator
CO_3^{2-}	Carbonate Ion
e^-	Electron
H^+	Hydrogen ion
O^{2-}	Oxygen Ion
CO_2	Carbon Dioxide
H_2O	Water
H_2	Hydrogen
O_2	Oxygen
A	Swept Area of Rotor Disc
I_{mpp}	Current at Maximum Power Point
I_{ph}	Light-Generated Current
I_L	Load Current
Jr	Inertia of the Shaft
P_{an}	Pressure Inside the anode Channel
P_r	Cell Pressure
R_{gass}	Gas Constant
V_{an}	Volume of the Anode
$OH - H^+$	Hydroxy Ion

List of Figures

List of Tables

Chapter 1

Introduction

1.1 Introduction

Recent developments in the electric utility industry are encouraging the entry of power generation and energy storage at the distribution level. Together, they are identified as distributed generation (DG) units. Several new technologies are being developed and marketed for distributed generation, with capacity ranges from a few kW to 100 MW. The DG includes microturbines, fuel cells, photovoltaic systems, wind energy systems, diesel engines, and gas turbines [1],[2] .

1.1.1 Definition of Microgrids

The Microgrid (MG) concept assumes a cluster of loads and microsources operating as a single controllable system that provides both power and heat to its local area. This concept provides a new paradigm for defining the operation of distributed generation [3],[4].

The microsources of special interest for MGs are small (<100-kW) units with power electronic interfaces. These sources are placed at customers sites. They are low cost, low voltage and have a high reliability with few emissions. Power electronics provide the control and flexibility required by the MG concept. A properly designed power electronics and controllers insure that the MG can meet the needs of its customers as well as the utilities. [1] defined characterstics of MGs as;

- Not centrally planned (by the utility)
- Not centrally despatched.
- Normally smaller than 50-100 MW.
- Usually connected to the distribution system.

Implementing an MG can be as simple as installing a small electricity generator to provide backup power at an electricity consumer's site, or it can be a more complex system that is highly integrated with the electricity grid that consists of electricity generation, energy storage, and power management systems. They comprise a portfolio of technologies, both on supply-side and demand-side, that can be located at or near the location where the energy is used. MG devices provide opportunities for greater local control of electricity delivery and consumption.

They also enable a more efficient use of waste heat in combined heat and power (CHP) applications, which boosts efficiency and lowers emissions. The CHP systems provide electricity, hot water, heat for industrial processes, space heating and cooling, refrigeration, and humidity control to improve indoor air quality and comfort.

Figure 1.1 shows the MG architecture. This consists of a group of feeders. There is a single point of connection to the main distribution utility called point of common coupling (PCC). SD means a Separation Device that can disconnect MG immediately when a fault occurs in the distribution grid. Some feeders, (feeders 1,2) have sensitive loads, which require local generation. The traditional loads are connected to Feeder 3 and do not have any local generation. Each of the local generation has a LC (local Controller). This is responsible for local control that corresponds to a conventional controller (ex. AVR or Governor) but that has a network communication function to exchange information between other LCs and the upper central controller to achieve an advanced control, The central controller also plays an important role as a central load dispatch control center in bulk power systems, which is in charge of distributed generator operations installed in MG [5].

MG technologies are playing an increasingly important role in the nation's energy portfolio. They can be used to meet baseload power, peaking power, backup power, remote power, power quality, and cooling and heating needs. Customers usually own small-scale, on-site power generators, but they may be owned and operated by a third party. If the distributed generator does not provide 100% of the customer's energy needs at all times, it can be used in conjunction with a distributed energy storage device or a connection with the local grid for backup power. The MG resources support and strengthen the central-station model of electricity generation, transmission, and distribution. The diagram below shows how the grid looks after the addition of distributed resources. Although the central generating plant continues to provide most of the power to the grid, the distributed resources meet the peak demands of local distribution feeder lines or major customers. Computerized control systems, typically operating over telephone lines, make it possible to operate the distributed generators as dispatchable resources that generate electricity as needed.

1.1.2 Reasons for Microgrids

The conventional arrangement of modern large power system offers a number of advantages. Large generating units can be made efficient and operated with only a relatively small number of personnel. The interconnected high voltage transmission network allows the generator reserve requirement to be minimized , the most efficient generating plant to be despatched at any time, and bulk power to be transported large distances with limited electrical losses. The distribution network can be designed for unidirectional flows of power and sized to accommodate customer loads only. However, over the last few years a number of influences have combined to lead to the increased interest in MGs schemes [1]. The policy drivers encouraging MGs are:

1. Reduction in gaseous emissions (mainly CO_2).
2. Energy efficiency or rational use of energy.
3. Deregulation or competition policy.

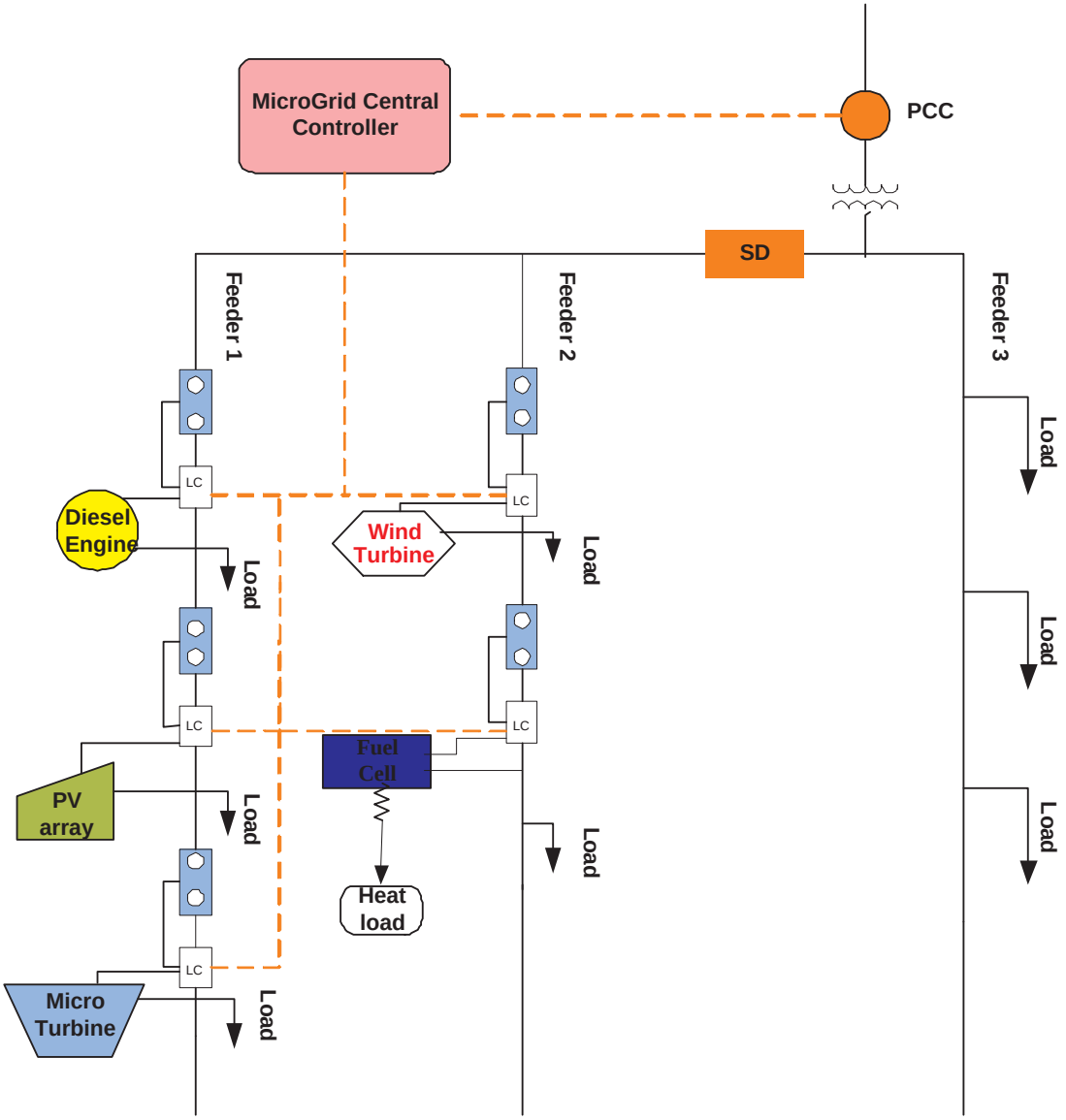

Figure 1.1: MicroGrid Architecture.

4. Diversification of energy sources.

5. National power requirement.

Reference [1] listed other reasons but with additional emphasis on commercial considerations such as:

- Availability of modular generating plants.
- Ease of finding sites for smaller generators.
- Short construction times and lower capital costs of smaller plants.
- Generating may be sited closer to load, which may reduce transmission costs.
- Technical impacts of Microgrids on the distribution system.
- Network voltage changes and regulation.

1.2 Motivation

Currently a lot of research is being undertaken into MGs and some model architectures have been proposed in the literature such as [3],[4],[6],[7],[8], [5] . Although the components of a MG are fairly well understood, the system as a whole is not. When several sources are connected to form a MG, the system behaviour is unpredictable. This being the case, modelling the system and simulating it in order to develop an appropriate control system, is the heart of micro-grid research. Nowadays several research groups around the world are investigating the feasibility and benefits that the MGs may provide. Some problems are encountered including dealing with unbalanced loads and harmonics associated with the system. This work does not intend to address such problems, rather it is concerned with the modelling of the MG for the investigation of the transient and steady-state response.

1.3 Technical Impacts of Microgrids on the distribution system

1.3.1 Network voltage changes and system regulation

Every distribution utility has an obligation to supply its customers electricity at a voltage within a specified limit. This requirement often determines the design and expense of the distribution circuit so that over the years techniques have been developed to make the maximum use of distribution circuits to supply customers within the required voltage [1]. Some distribution utilities use more sophisticated control of the on load tap changers of the distribution transformer by regulators on the feeder and including the use of the current signal compounded with the voltage measurement at the switched capacitor on feeders [9]. Feeding power from a Distribution Generator (DG) unit can cause negative impacts on the network voltage in case a DG unit is placed just downstream to a load tap-changer transformer [10]. In this case, the regulators will not correctly measure the feeder demands. Rather, they will see lower values since the DG unit reduces the observed load due to the onsite power generation. This will lead to setting the voltage at lower values than that required to maintain adequate levels at the tail ends of the feeder [10]. However, the most favourable locations of DG units near the end user terminals can provide the required voltage support at the feeder nodes.

1.3.2 Increase of network fault levels

Most of the MG plants use rotating machines and these will contribute to the network fault levels. Both induction and synchronous generators will increase the fault level of the distribution system although their behaviour under sustained fault conditions differs.

The fault level contribution can be reduced by introducing impedance between the generator and the network by a transformer or reactor but at the expense of increased losses and wider voltage variations at the generator [1].

In urban areas where the existing fault level approaches the rating of the switchgear, the increase in fault level can be a serious impediment to the development of Distributed Generation.

1.3.3 Power quality

Two aspects of power quality are usually considered to be important: (i) transient voltage variations and (ii) harmonic distortion of the network voltage [1]. The MG can cause transient voltage variations on the network if relatively large current changes during connection and disconnection of the generator are allowed. Therefore, it is necessary to limit voltage variations to restrict the light variation. Generally, load fluctuation can cause voltage variation as well as source fluctuation [11]. MG units have the potential to cause unwanted transient voltage variations at the local power grid. Step changes in the outputs of the MG units with frequent fluctuations and the interaction between the MG and voltage controlling devices in the feeder can result in significant voltage variations [9]. The standalone operation of MG units gives more potential for voltage variations due to load disturbances, which cause sudden current changes to the DG inverter. If the output impedance of the inverter is high enough, the changes in the current will cause significant changes in the voltage drop, and thus, the AC output voltage will fluctuate. Conversely, weak ties in the grid integration mode give a chance for transient voltage variations to take place but lower degrees than in the standalone mode [10].

Incorrectly designed or specified MG plants, with power electronic interfaces to the network, may inject harmonic currents, which can lead to an unacceptable network voltage distortion. The type and severity of these harmonics depend on the power converter technology, the interface configuration, and mode of operation [12]. Fortunately, most new inverters are based on Insulated Gate Bipolar Transistor (IGBT), which uses Pulse Width Modulation (PWM) to generate quasi-sine wave [9]. Recent advances in semiconductor technology enable the use of higher frequencies for carrier wave, which result in quite pure waveforms [10].

1.3.4 Protection

A number of different aspects of MG protection can be identified [1]:

- Protection of the generation equipment from internal faults.
- Protection of the faulted distribution network from fault currents supplied by the MGs.
- Anti-islanding or loss-of-mains protection.
- Impact of MGs on existing distribution system protection.

1.3.5 Stability

For Distributed Generators schemes, the objective of which is to generate power from new renewable energy sources, considerations of generator transient stability tend not to be of great significance. If a fault occurs somewhere in the distribution network to depress the network voltage and the Distributed Generator trips, then all that is lost is a short period of generation. The MGs will tend to overspeed and trip on their internal protection. The control scheme in the MGs will then wait for the network condition to be restored and restart automatically. In contrast, if a DG is viewed as providing support for the power system, then its transient stability becomes of considerable importance. Both voltage and/or angle stability may be significant depending on the circumstances.

1.4 Objectives of the Thesis

This thesis aims to model MGs at steady state and study their transient responses to changing inputs. The MG components which have been studied are the Diesel Engine, the Fuel Cell, the Microturbine, the Wind turbine, and finally the Photovoltaic Cell. It is intended that the work completed in this thesis will lay the ground work for further model development. The long term goal is to have of a highly sophisticated, complete model of a MG, so as to allow for a full understanding of how MGs behave. The goal of this thesis is to build a complete model of a MG including the power sources, their power electronics, a load and mains model in MATLAB/Simulink.

1.5 Outline of the Thesis

The work in this thesis is organized as follows.

In Chapter 1, an introduction and a background is presented of Distributed Generator (DG) units and their potential impact on power systems. The main focus in Chapter 2 is on the modelling and speed control of the Diesel Engine using Genetic Algorithm Self Tuning PID Controller. An investigation on the dynamic modelling of a Fuel Cell as a promising DG unit, and its performance are introduced in Chapter 3. The objective of Chapter 4 is to investigate the impact of the power demand on a Microturbine model and study the responses such as current and voltage and output power. Chapter 5 deals with the wind turbine, by examining its behavior when the wind speed changes.

Photovoltaic Cell is modeled and its the performance for different irradiance and various temperatures conditions is investigated in Chapter 6. Finally, conclusions and future consideration are summarized in Chapter 7

Chapter 2

Diesel Engine Modeling and Speed Control

2.1 Introduction

Diesel Engines, developed more than 100 years ago, were first among distribution generator technologies. Both Otto (spark ignition, SI) and Diesel cycle (compression ignition, CI) engines have gained widespread acceptance in almost every sector of the economy. Because of their high efficiency and reliability they are used on many scales, ranging from small units of 1 KW to large several tens of MW power plants. Smaller engines are primarily designed for transportation and can usually be converted to power generation with little modification. Large engines are most frequently designed for power generation, mechanical drive, or marine propulsion. Because of sudden changes in load demands by the consumers, it is important that the diesel prime mover has a fast dynamic response and good capabilities of disturbance rejection [13].

Almost all diesel engines used for power generation are four-stroke and operate in four cycles (intake, compression, combustion, and exhaust). The process begins with fuel and air being mixed. In turbo-charged applications, the air is compressed before mixing with the fuel. The fuel/air mixture is introduced separately with fuel being injected after the air is compressed [13], [1].

The Diesel Engine model gives a description of the fuel consumption rate as a function of speed and mechanical power at the output of the engine, and is usually modeled by a simple first order model relating the fuel consumption (fuel rack position) to the engine mechanical power [14].

The power output of the engine and the generator has to be varied with the changing load in order to meet the consumer demands. The task of the governor is to adjust the fuel flow and then regulate the input of the engine and generator hence provide the required power to meet the change in the load.

The presence of the dead-time between the actuator fuel injection and the production of mechanical torque is a very important characteristic of the diesel engine. The dead time is an unknown time delay and is commonly considered as a complicated function of operating conditions and engine speed [15]. There are also system parameter uncertainties with the dead time rise; a control problem which significantly degrades the performance of the prime mover,

especially under load presence.

A Diesel Engine is a nonlinear system because of the existence of a nonlinear, time-varying dead time between the injection and production of the mechanical torque, which can be represented by a gain and a dead time. The model is commonly used in conjunction with a PI controller to prevent the steady-state error in speed [16]. A lot of research has been carried out on the diesel prime-mover. In [17] adaptive control was proposed to control the speed, in [18] neural network and fuzzy logic were applied for modeling and simulation of the diesel driven stand alone power generating system. The H_∞ controller has been proposed for diesel engine systems in [15]. In [19] the author compares the performance of a k- predictive adaptive control with fixed PI control scheme.

In this work to estimate the time-varying parameters of the diesel engine system, a Recursive Least Squares (RLS) estimator and an indirect estimation scheme for dead time will be implemented. This will provide an up-to-date estimate of the system for the Genetic algorithm to determine the optimum PID controller, with the use of an objective function that evaluates the optimum PID gains based on the controlled systems overall error. The Recursive Least Squares estimator will then be defined to estimate the parameter variations of the diesel engine system to provide the most accurate estimation of the system for the genetic algorithm to design a PID controller. Simulation results indicate that the genetic algorithm overcomes many difficulties such as rise time, overshoot, and load handling, etc; and produces satisfactory results for controlling the speed of the diesel engine in the start up and when loads are applied.

Our goal is to propose an objective function to find a PID controller that gives small overshoot, fast rise time, and quick settling time. In order to combine all of these objectives, a proper objective function will be set up that will minimize the error of the controlled system.

2.2 Modelling of Diesel Engine

There are many methods already proposed for modelling the diesel generator [14], [15], [16], [17], [5]. From control system point of view, a diesel engine can be considered as a speed-feedback system. After the operator gives a speed command through adjusting the governor setting, the engine governor which is also working as a sensor, will recognize the difference between the actual speed and the desired speed, and regulates the fuel supply to maintain the engine speed within range.

The general structure of the fuel actuator system is usually represented as a first order phase-lag network, which is characterized by gain K_2 and time constant τ_2. Figure 2.1, and equation (2.1) shows the actuator and the current driver constant K_3 . The output of the actuator is the fuel-flow $\Phi(s)$ and the input current is $I(s)$

$$\Phi(s) = \frac{K_3 K_2}{(1 + \tau_2 s)} I(s) \tag{2.1}$$

Fuel Flow $\Phi(s)$ is then converted into mechanical torque $T(s)$ after a time delay τ_1 and engine torque constant K_1, which can be represented by the model as shown in Figure 2.2, and equation (2.2).

$$T(s) = \Phi(s) K_1 e^{-\tau_1 s} \tag{2.2}$$

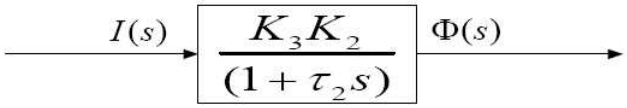

Figure 2.1: The Actuator Model and the current driver constant.

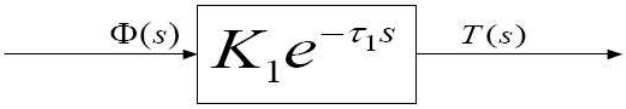

Figure 2.2: The Engine Model.

The governor can be defined as a mechanical or electromechanical device for automatically controlling the speed of an engine by relating the intake of the fuel. Several types of governors exist such as mechanical-hydraulic, direct mechanical, electro-hydraulic, electronic, and microprocessor based [14].

The flywheel represents the complex dynamic effects of the engine inertia, the angular speed of a flywheel ω_w , the viscous friction coefficient ρ, and the loaded alternator. Its model is assumed to have an integrator with flywheel acceleration constant J which serves to filter out a large proportion of the disturbance and noise effects. The noise itself is an inherent property of all internal combustion engines. As proposed in [15], an integrator is added between the reference signal r and the engine actuator. It is necessary to eliminate the speed droop in steady-state operation by raising the order of the whole system as shown in Figure 2.3. However in our simulation work, we obtain additional improvements to the results without using the integrator. The typical set of per unit values used in the simulation is taken from [15] and

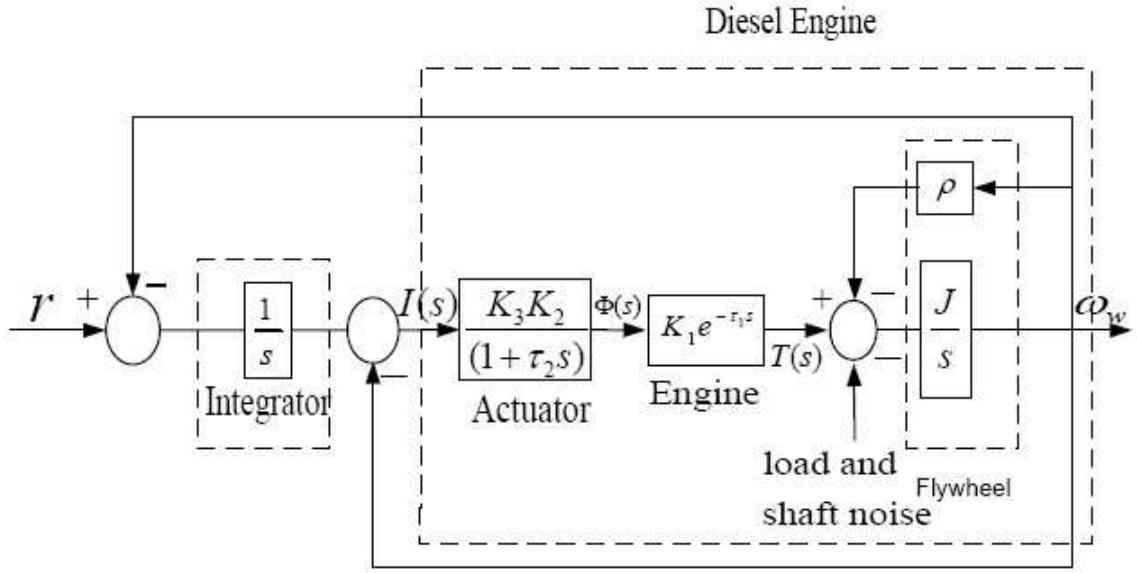

Figure 2.3: The Block diagram of the Diesel Engine System.

[19] as indicated in Table 2.1.

The values of K_3 and K_2 can be considered to be constant for a particular engine setup. Gain K_3 is a factor that determines the amount of the mechanical torque obtained per unit of fuel flow. It depends on the operating point of the prime mover. Time constant τ_2 is quite dependent on the temperature of the oil flowing into the actuator. Both K_2 and τ_2 are variable, but the variation is negligible in a small time interval, [15].

As seen from Figure 2.2 and from literature such as [15], [17], [18] and [19], the engine combustion system is commonly represented by the engine torque constant multiplied by a time delay . In a real system, the dead time is mainly comprised of three components:

1. The time from the actuator signal change until fuel is injected to any cylinder. This is called "power stroke delay".
2. The time for the fuel to burn in a cylinder and to produce a torque output, which is similar to the characteristic "combustion delay".
3. The time for a new torque level to produce a sufficient number of cylinders to assignable to the prime-mover as a whole. This is an effect of the multi cylinder nature of the prime-mover.

The complete parameter range values for the diesel engine system are given in [15] and restated in Table 2.1.

Table 2.1: System Parameters of a Typical Diesel Engine .

System parameters	Value range	Nominal values
Actuator gain constant K_2 (per unit)	1.0	1.0
Actuator time constant τ_2 (s)	$0.05 \sim 0.2$	0.125
Engine torque constantK_1 (per unit)	$0.8 \sim 1.5$	1.15
Current driver constant K_3 (per unit)	1.0	1.0
Engine dead time τ_1 (s)	$0 \sim 1.0$	0.5
Plant and flywheel acceleration $J(s^{-1})$	$0.1 \sim 0.5$	0.3
Friction coefficient ρ(per unit)	0.1	0.1

The speed of the power generation plants driven by diesel prime movers is difficult to control optimally using a PID controller because the system parameters are changing.

2.2.1 System Description

The actuator-engine system to be considered is from Figure 2.3 :

$$G(s) = \frac{T(s)}{I(s)} = \frac{K_0}{s(1+\tau_2 s)} e^{-\tau_1 s} \tag{2.3}$$

where the actuator time constant is τ_2, engine time delay τ_1, and the process gain $K_0 = K_1 K_2 K_3$. The parameters are usually unknown or time varying.

First order Pade approximation for the time delay term yields:

$$e^{-\tau_1 s} \approx \frac{1 - \tau_1/2}{1 + \tau_1/2} \tag{2.4}$$

The following simplified transfer function can now be obtained from (2.3):

$$G'(s) = \frac{K_0}{s(1+\tau_2 s)} \frac{1-\tau_1/2}{1+\tau_1/2} \tag{2.5}$$

The discrete time model corresponding to equation (2.5) can be expressed as:

$$A(z^{-1})y(t) = B(z^{-1})u(t-1) + \zeta(t) \tag{2.6}$$

where $u(t)$ is the system input (current), $y(t)$ is the system output (torque), and $\xi(t)$ is an uncorrelated zero main random sequence. Time t takes usually discrete values $t = 0, 1, 2, ...$

In (2.6) A and B polynomials are

$$\left.\begin{array}{l} A(z^{-1}) = 1 + a_1 z^{-1} + a_2 z^2 + ... + a_{n_1} z^{-n} \\ B(z^{-1}) = b_0 + b_1 z^{-1} + b_2 z^{-2} + ... + b_m z^{-m} (b_0 \neq 0) \end{array}\right\} \tag{2.7}$$

where z^{-1} is the backward shift operator. The order of the polynomial $A(z^{-1})$ is n and that of $B(z^{-1})$ m,.

2.2.2 Parameter estimation

The parameter estimation algorithm is based on an exponentially weighted sequential least squares method, [20], which is summarized in (2.8)-(2.14).

$$\hat{\theta}(t) = \hat{\theta}(t-1) + K(t)(y(t) - \varphi^T(t)\hat{\theta}(t)) \tag{2.8}$$

where the gain

$$K(t) = \frac{P(t-1)\varphi(t)}{\gamma + \varphi^T P(t-1)\varphi(t)} \tag{2.9}$$

error covariance

$$P(t) = M(t)\left\{\frac{1}{\gamma}(P(t-1) - K(t)\varphi^T(t)P(t-1))\right\}M(t) \tag{2.10}$$

$$M(t) \equiv diag\left\{\frac{1}{m_i(t)}\right\}(i = 1, ..., N, N = n + r + 1, 0 < m_i \leq 1) \tag{2.11}$$

$$m_i(t) \equiv \sqrt{1 - \frac{(y(t) - \varphi^T(t)\hat{\theta}(t-1))^2 g_i}{1 + \varphi^T(t)P(t-1)\varphi(t)}}(i = 1, ..., N) \tag{2.12}$$

and

$$\theta^T = [a_1....., a_n, b'_0, ..., b'_r] \tag{2.13}$$

is the parameter vector, and

$$\varphi^T(t) = [-y(t-1), ..., -y(t-n), u(t-\tau_{\min}), ..., u(t-m-\tau_{\min})] \tag{2.14}$$

is the data vector.

γ is the forgetting factor, g_i is the factor of adaptive sensitivity. If the designer sets g_i to too large a value the corresponding parameter will be more sensitive. The estimation of parameters

$b'_0 \sim b'_r$, including the dead time of the plant, is more sensitive than that of $a_1 \sim a_n$ so that $g'_i s$ are set up in the following manner:

$$g_1 \sim g_n < g_{n+1} \sim g_{n+r+1} \tag{2.15}$$

Moreover, when the variation of the estimation parameters is too high at the point of initial control step or when the dynamic characteristics of the system are changed; the control input assumes an excessively large value. Then, in order to reconstitute the controller, we employ a renewal condition to apply the estimated parameters. Concretely, when the variation of the estimated parameters is more than the previous one by 50% or $B'(1)$ of equation (2.5) has a very small value, the estimated parameters are stopped being updated.

Since the diesel engine system that is to be estimated is part of the control loop, an additional problem is introduced. The feedback signal may cause an interruption in the relationship between the input and the output signal causing the RLS estimator to malfunction. The most effective way to tackle this problem is to add an independent signal into the loop. This extra dither signal should satisfy the requirement for persistent excitation and should not have large amplitude components that could drive the system into non-linear operation [21]. We have used Pseudo Random Binary Signal (PRBS) because it only has two amplitude levels that may be selected so that the amplitude does not exceed the bands of linearity of the system. The main advantage of the PRBS is that it has a rich spectrum and is an ideal input for the system to be estimated.

2.2.3 Indirect estimation of dead time

In this work we will use indirect estimation for the dead time explained in [20]. It is difficult to estimate the dead time directly from an unknown time-delay system. Using a complex algorithm tends to increase the computational burden, and so it is desirable to apply a straightforward method in discrete time for this problem. The estimation of an unknown time delay is included in the estimation of parameters of $B(z^{-1})$ in (2.7). The modified polynomial $B'(z^{-1})$ is given by:

$$\begin{aligned} B'(z^{-1})z^{-\tau_{1\min}} &= (b'_0 + b'_1 z^{-1} + \text{.....} + b'_r z^{-r})z^{-\tau_{1\min}} \\ &= B(z^{-1})z^{-\tau} \end{aligned} \tag{2.16}$$

where $r = m + \tau_{1\max} - \tau_{1\min}$, $\tau_{1\max}$ and$\tau_{1\min}$ are the lower and upper limit values of the dead time, respectively and τ_1 is the dead time of the system . When the estimated parameters $b'_0 \sim b'_r$ of equation (2.5) have converged, the obtained data are expected to have the following character:

$$\begin{aligned} b'_i &= \varepsilon(i \leq \tau - \tau_{1\min} - 1) \\ b'_j &= \varepsilon(j \geq \tau - \tau_{1\min} + m + 1) \end{aligned} \tag{2.17}$$

where ε is a very small value. Therefore, it is possible to estimate the dead time of the plant using this character without complex calculations.

2.3 Controller Design

The controller most commonly used in feedback applications is the PID (proportional, integral, derivative) controller. There have been a few studies about tuning PID controllers for system with varying time delays. The robust control framework has been used to treat variations in the delay, also time-varying delays have received attention by solving the linear- quadratic problem for time varying delay [22]. In [22], an optimal tuning method for PID controllers with time-varying delays was considered where PID controller parameters are presented as a function of the process time constants. An ingenious transformation is presented in [23] to develop a time-varying PID controller for flow processes.

2.3.1 PID Controller

The conventional PID controller is the most widely used controller in industry due to its simple control structure, ease of design, and inexpensive cost. However, the PID controller cannot give a good control performance if the controlled object is highly nonlinear and contains uncertainties.

The proportional controller output uses a 'proportion' of the system error to control the system. This introduces an offset error into the system. In case of the integral controller,its output is proportional to the amount of time there will be an error present in the system. The integral action removes the offset introduced by the proportional control but introduces a phase lag into the system. In the derivative controller, output is proportional to the rate of change of the error. Derivative control is used to reduce/eliminate overshoot and it introduces a phase lead action that removes the phase lag introduced by the integral action. The velocity-type discrete-time PID control law used in this study is described as:

$$\Delta u(t) = \frac{k_c T_s}{T_I} e(t) - k_c(\Delta + \frac{T_D}{T_s}\Delta^2) y(t), t = 0.1, 2, ... \tag{2.18}$$

where $u(t)$ is the control variable, $e(t)$ the control error signal defined as $e(t) = y_{ref}(t) - y(t)$,$y_{ref}(t)$ is the reference value, and $y(t)$ is the output of the system.Δ denotes the differential operator defined by $\Delta := 1 - z^{-1}$. Parameters k_c ,T_I and T_D are the proportional gain, integral and the derivative time, respectively.

2.3.2 Genetic Algorithms

In their original and most basic form, genetic algorithms (GA) were designed as objective search and optimization algorithms. The GA starts with no knowledge of the correct solution and depends entirely on responses from its environment and evolution operators to reach the best solution. The GA have been recognized as a powerful tool in many control applications such as parameter identification and control structure design [24] , [25], [26] , [27]. GA differs substantially from more traditional search and optimization methods. The four most significant differences can be summarized as:

1. GA searches a population of points in parallel, not a single point.

2. GA does not require derivative information or other auxiliary knowledge; only the objective function and corresponding fitness levels influence the directions of search.

3. GA uses probabilistic transition rules, not deterministic ones.
4. GA works on an encoding of the parameter set rather than the parameter set itself (except where real-valued individuals are used).

The GA proceeds as follows:

Reproduction or fitness determination

The first step is to set up a population of chromosomes, evaluate a fitness function for each chromosome and subsequently grade them. The value of the fitness function is used in the selection process to provide a bias towards fitter individuals. The PID gains are obtained by evaluating the cost function for each individual and decoding the string which is then applied to the Simulink model for the closed-loop system.

Selection

Selection is the process of determining the number of times an individual will be chosen for reproduction and the number of offsprings that an individual will have. There are two separate steps in the selection of the individual:

1. Determine of the number of times an individual can expect to be chosen.
2. Conversion of the expected number of trials into a discrete number of offspring.

Part one is concerned with the conversion of raw fitness values into real-valued expectations of probability that the individual will reproduce. Part two is a probabilistic selection of individuals for reproduction based on the fitness of an individual relative to each other. This is an elitist strategy that ensures that the next generation's best will never degenerate and hence guarantees the asymptotic convergence of the GA. Normalized geometric selection is the primary selection process to be used in this work. The GAOT toolbox [28] provides two other selection functions, Tournament selection and Roulette wheel selection. Tournament selection has a longer compilation time than the rest and as the overall run time of the genetic algorithm is an issue. The roulette wheel option is inappropriate because it is not implausible for the weakest string to determine the selection process. When using the normalized geometric selection, the only parameter that has to be declared is the probability of selecting the fittest chromosome of each generation. In this thesis the probability is set to 0.08.

Crossover

Crossover is the basic operator for producing new individuals in genetic algorithms. Just like nature, the offspring will have certain characteristics of the two parent strings.

Arithmetic crossover was chosen as the crossover procedure. Single point crossover is too simplistic to work effectively on a chromosome with three alleles, a more uniform crossover procedure throughout the chromosome is required. Heuristic crossover was discarded because it performs the crossover procedure a number of times and then picks the best one. This increases the compilation time of the program and is undesirable. The arithmetic crossover procedure is specifically used for floating point numbers and is the ideal crossover option for use in this study.

Mutation

In natural evolution, mutation is a random process that causes one part of a gene to change which results in an entirely new genetic structure. Mutation in genetic algorithms, like its counterpart in nature, occurs with a low probability - typically in the range from 0.001% to 0.01%. The role of mutation is thought to have two main functions; firstly, it provides a guarantee that the probability of searching any given string will never be zero and secondly to act as a safety net to recover good genetic material lost through the operations of selection and crossover. The Multi non-uniformly distributed mutation operator, was chosen as the mutation operator as it is considered to function well with multiple variables. The mutation operator has three options when the multi non-uniformly distributed mutation function is used. The first is the total number of mutations, normally set with a probability of around 0.1%. The second parameter is the maximum number of generations and the third parameter is the shape of the distribution. This last parameter is set to a value of two, three, or four, where the number reflects the variance of the distribution. The simulation and the genetic algorithm routine were implemented using The MATLAB/ Simulink environment, with the GA Toolbox [28].

The genetic algorithm was initialized with a population of 20 and iterated for 100 generations. The bounds of the genetic algorithm reduced to a smaller range of numbers. This ensured quick convergence and a reduction in the number of generations necessary for the algorithm to converge to optimum PID gain values, which in turn will reduce the overall runtime of the genetic algorithm

The genetic algorithm code simulated the Simulink file, which includes the plant, and the RLS estimator (S-Function). The genetic algorithm takes in the parameter estimates and then performs the genetic algorithm search. The genetic algorithm then updates the PID controller and reads in the parameter estimates.

To ensure that the GA tuned controller produces a stable overall system, additional code was added that analyzed the stability of the controlled system. The stability of the system was examined by accessing the magnitude of the real and imaginary parts of the discrete poles.

2.4 Self Tuning PID controller based Genetic Algorithms

The speed loop control study involves two types of changes on the performance conditions, startup and load disturbances. For the purpose of performance studies, the diesel prime mover with a genetic algorithm self tuning PID controller has been simulated. In the startup condition a unit step signal is applied at t=0 and after 25 s another unit step signal was injected as a load disturbance to see how the controller reacts.

In order to see the performance of the system as time delay varies, the time delay is varied from 0.0s to 0.25s with nominal system parameters. For the uncertainty test of the system parameters, three sets of parameters were used, i.e, the maximum ($\tau_2 = 0.2s, K_1 = 1p.u, J = 0.3s^{-1}, \tau_1 = 0.125s$), minimum ($\tau_2 = 0.05s, K_2 = 0.8p.u, J = 0.1s^{-1}, \tau_1 = 0.125s$), and nominal($\tau_1 = 0s$, $0.125s$, and $0.25s$).

The procedure will be as follows:

1. Estimate $\hat{\theta}(t)$ by using the RLS algorithm in (2.8)- (2.14).

2. Estimate the dead time using indirect estimation .
3. Form the discrete model of the diesel engine using the parameters determined in steps 1 and 2.
4. The GA automatically simulates the Simulink file.
5. Tune PID parameters using GA.
6. If the error tolerance for design parameters are met then go to step 8.
7. Update $t \rightarrow t + 1$ and return to step 1.
8. Stop.

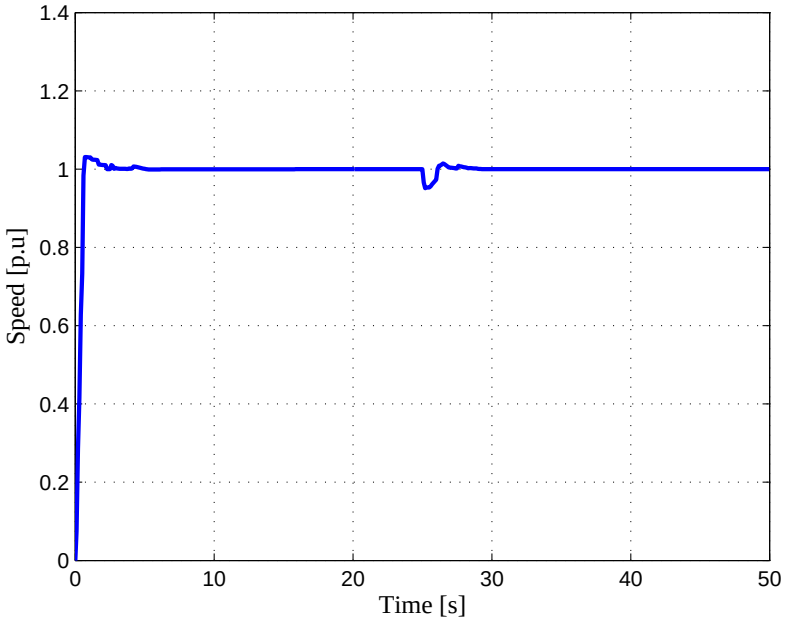

Figure 2.4: Unit step response of the studied diesel engine under time delay $\tau_1 = 0s$

2.5 Simulation Results

In this section we will discuss the simulations of the diesel engine with the proposed controller which has been carried out under various conditions.

The simulation of the startup condition can be done by adding a unit step signal to the reference input. The startup studies are important for oil engines because generating units driven by them are usually used to supplement other main units at time of peak load. Unlike other commercial prime movers, the diesel engine must prosses a good dynamic response at start up. In practice, the prime mover is usually driven to a low speed level using starter motors of some kind [19].

For a sudden load change, which in practice may occur due to electrical faults on the alternator side, another unit step signal is injected to the disturbance input to simulate the load disturbance situation.

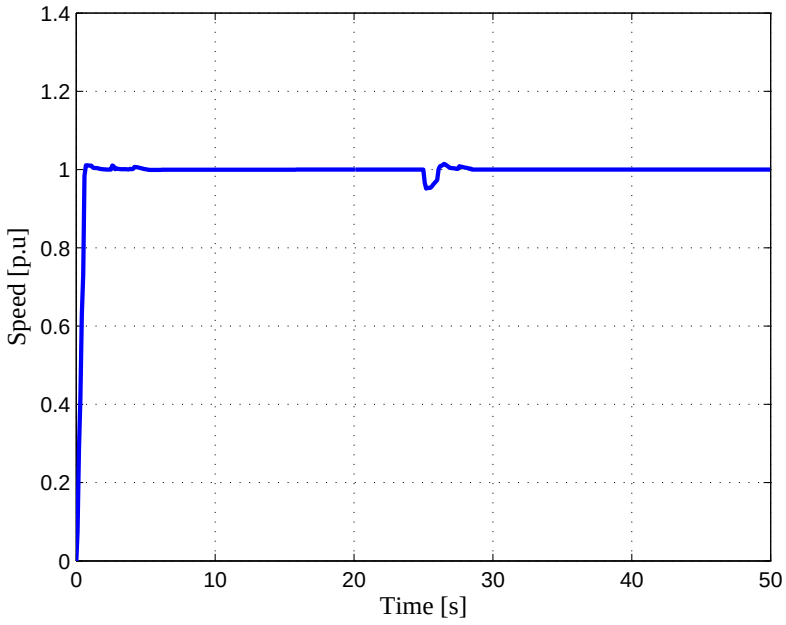

Figure 2.5: Unit step response of the studied diesel engine under time delay $\tau_1 = 0.125s$

Figures 2.4, 2.5, and 2.6 show the unit step responses of the diesel system under the nominal system parameters.The time delay was chosen to be $\tau_1 = 0s$, $0.125s$, and $0.25s$ respectively.

There was clear improvement in the unit step response compared to the works [15], [17], and [19] in the overshoot and settling time at the start up due to fast computing.

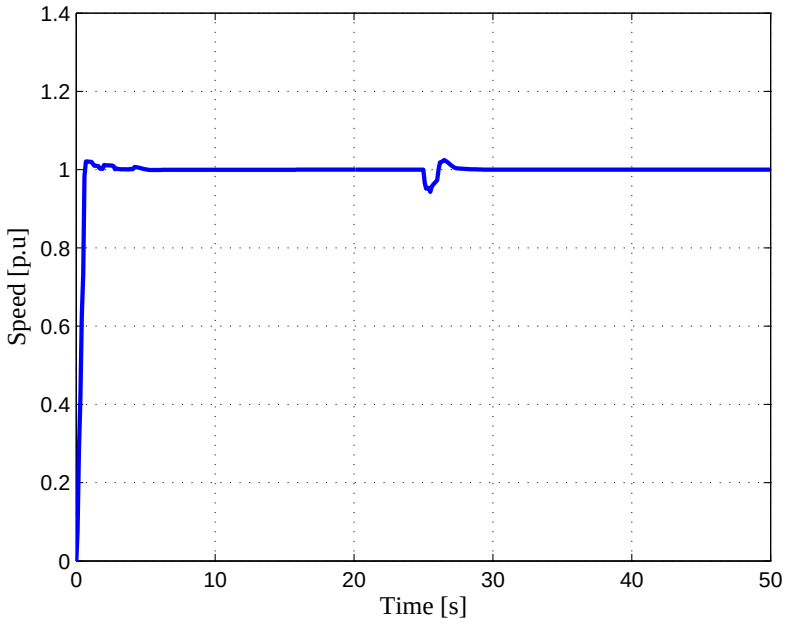

Figure 2.6: Dynamic response of the diesel engine under time delay $\tau_1 = 0.25s$

The overshoot decreased and the settling time was also about less than 5 s for all the variations of time delay τ_1. There was slight improvement in the load handling of the proposed controller. The overshoot and settling times were very satisfactory, and the controller performed

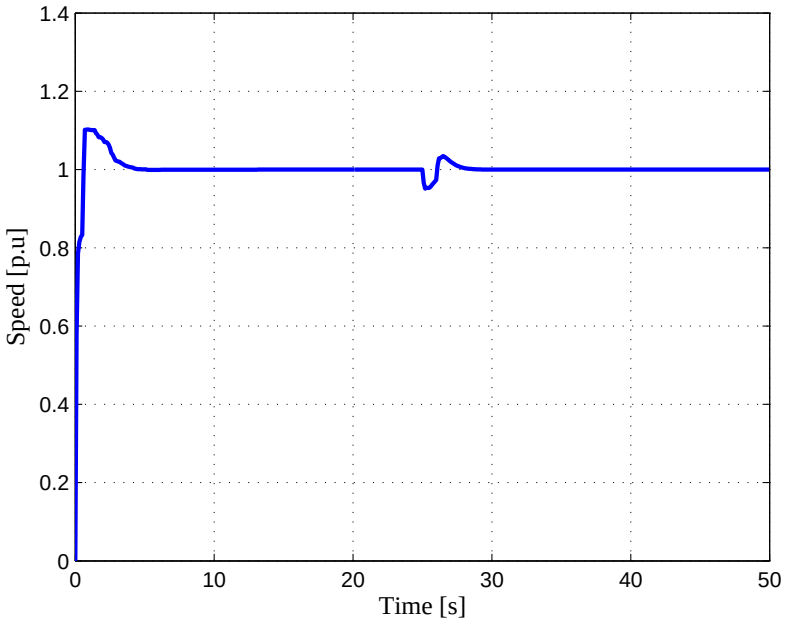

Figure 2.7: Response under the minimum set of parameters,$\tau_2 = 0.05s, K_2 = 0.8p.u, J = 0.1s^{-1}, \tau_1 = 0.125s$

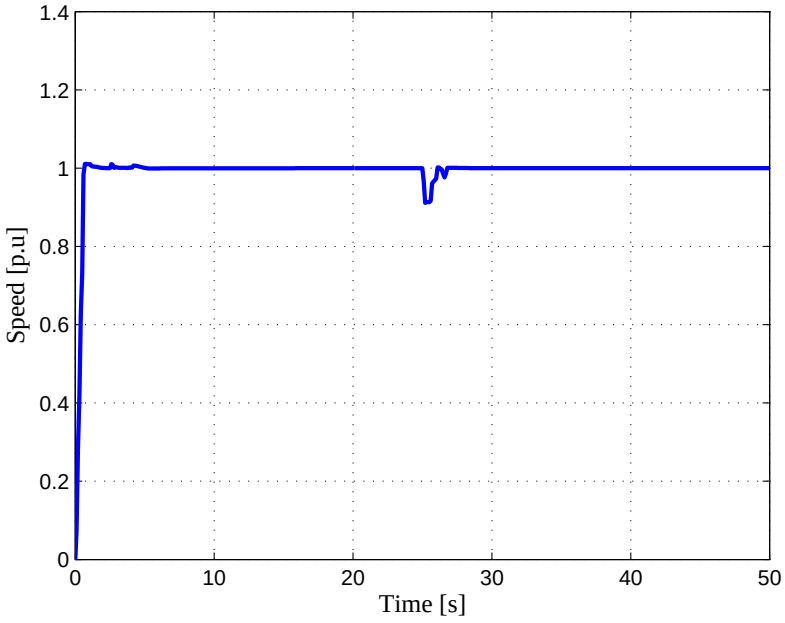

Figure 2.8: Response under the maximum set of parameters $\tau_2 = 0.2s, K_1 = 1p.u, J = 0.3s^{-1}, \tau_1 = 0.125s$

in the same good way for all the variations of the time delay. When the dead time reached the upper bound,$\tau_1 = 0.25s$, in Figure 2.6, the controller produced very small overshoot and the settling time was less than 5 s.

Additionally in Figures 2.7, 2.8, there were improvements related to overshoot and settling time for the start up and when the load for both lower bounds and upper bounds were applied.

Chapter 3

Fuel Cell

3.1 Introduction

Fuel cells generate power through the electrochemical reaction between hydrogen and oxygen. The conversion is highly efficient and leaves only water and heat as by-products, which is the main motivation for the increasing interest in the technology [29]. Fuel Cells offer lower emission and higher efficiency than Diesel Engine but are likely to be expensive for many applications. The first fuel cell unit was discovered and developed by Sir William Grove 1842 [30] with the use of four primitive cells utilizing hydrogen and oxygen. However, it was not practically used until the 1960's when NASA demonstrated a potential fuel cell application. After such demonstrations, commercial companies became interested in this technology because of its power quality, high efficiency, modularity, and environmental benefits.

Fuel cells could potentially replace the internal combustion engine and many other energy generation devices used today. Reduced emissions of greenhouse gases and increased efficiency are two of the major reasons that fuel cells are being seriously researched as a replacement to the internal combustion engine. This work presents an overview of fuel cell systems, their applications, their benefits and challenges, an explanation of the need for a transient analysis of fuel cell systems, and an overview of the relevant background literature.

A fuel cell (FC) is an electrochemical energy conversion system, where chemical energy is converted directly into electrical energy and heat. Resulting advantages of this technology are high efficiency almost at partial load, low emissions, and noiselessness (due to nonexistence of moving parts), and free adjustable ratio (50 kW to 3 MW) of electric and heat generation. The basic structure of fuel cells consists of a pair of electrodes and an electrolyte. The fuel which is usually hydrogen, is supplied to the anode where the fuel then is oxidized, yielding electrons, which move through the external circuit. At the cathode, the oxidant is reduced, consuming electrons from the external circuit. Ions move through the electrolyte to balance the flow of electrons through the external circuit. The anode-cathode reactions and the composition and direction of flow of the mobile ion vary with the type of fuel cell.

Figure 3.1 explains the operation principle, cathode reactions, and the mobile ion associated with most common fuel cell types.

The reactions of Alkaline Fuel Cell (AFC), Proton Exchange Membrane Fuel Cell (PEMFC), Phosphoric Acid Fuel Cell (PAFC), Molten Carbonate Fuel Cell (MCFC) and Solid Oxide Fuel Cell (SOFC) are summarized in Table 3.1.

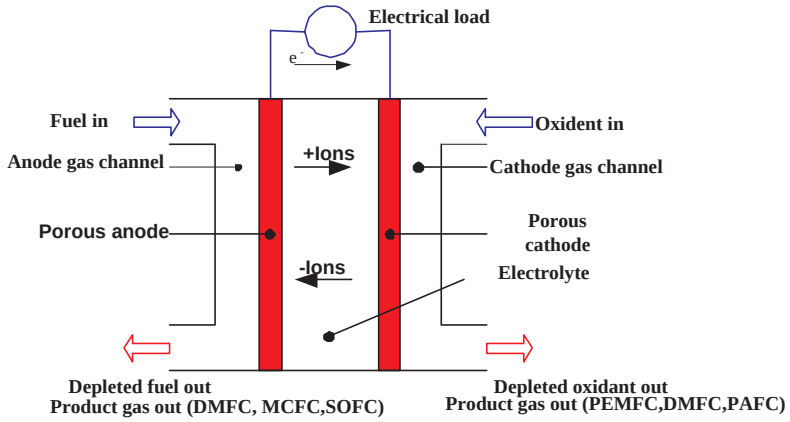

Figure 3.1: Operation principle, cathode reactions, and the mobile ion associated with most common fuel cell types.

Table 3.1: Summary of chemical reactions in different types of fuel cell.

Fuel cell type	Anode reaction	Mobile Ion	Cathode reaction
PEMFC and PAFC	$H_2 \rightarrow 2H^+ + 2e^-$	H^+	$1/2O_2 + 2H^+ + 2e^- \rightarrow H_2O$
AFC	$H_2 \rightarrow 2H^+ + 2e^-$	OH^-	$1/2O_2 + H_2O + 2e^- \rightarrow 2OH^-$
MCFC	$H_2O + CO_3^{2-} \rightarrow H_2O + CO_2 + 2e^-$	CO_3^{2-}	$1/2O_2 + CO_2 + 2e^- \rightarrow CO_3^{2-}$
SOFC	$H_2 + O^{2-} \rightarrow H_2O + 2e^-$	O^{2-}	$1/2O_2 + 2e^- \rightarrow O^{2-}$

CO_2: - carbon dioxide e^-: - electron H_2O:- water CO_3^{2-}: - carbonate ion H_2: - hydrogen

OH- H^+:- hydroxy ion H^+: - hydrogen ion O_2 - oxygen O^{2-}: - oxygen ion

3.1.1 Characteristics

There are four major fuel cell technologies with somewhat different characteristics. The main apparent difference is the electrolyte, which also has far reaching effects on the design and operating characteristics of the fuel cell. In Table 3.2. those four technologies are listed with some key characteristics.

Table 3.2: Major fuel cell technologies.

	PEMFC (PEFC)	PAFC	MCFC	SOFC
Electrolyte	Protone Exchange Membrane	Phosphoric Acid	Molten Carbonate	Solid Oxide
Operating temperature (^oC)	80	200	650	800-1000
Electric efficiency based on natural gas*(%)	30-35	35-40	45-55	45-55

*With hydrogen as fuel the electric efficiency is the same or even higher for low temperature fuel cells, as this is not a Carnot process. The reason for the higher efficiency with higher temperature for natural gas (or any reformed fuel) lies primarily in that fuel processing can be thermally integrated with the fuel cell and to a lesser extent to lower internal electric resistances.

All fuel cells generate a direct current, the voltage depending on cell voltage and the number of cells in series. Furthermore, the voltage varies with the load and also to some extent with time as the fuel cell stack ages. To obtain AC current, the equipment should have power-conditioning equipment to handle DC to AC conversion and current, voltage, and frequency control. Apart from supplying power to the external point of supply, the fuel cell also has to cover some internal power needs, e.g. pumps, fans, and control system.

As fuel cells are in a development stage, it is difficult to make general statements about operating characteristics as, for example, operating procedures tend to be on the cautionary side. Tentatively the following characteristics can be listed:

1. Start-up time depends on type of fuel cell and type of fuel processing system. A low temperature fuel cell (PEMFC) with partial oxidation could probably be started in a couple of minutes while a high temperature fuel cell takes 3 to 4 hours due to the need of avoiding thermal stresses during warm up. Generally speaking, high temperature fuel cells are not suited for start-stop operation.

2. A fuel cell in itself can facilitate nearly instant load changes. However, a fuel cell system has a limiting factor in the fuel processing system which has a certain time lag (varying depending on the type) and a truly load following system would need a buffer, e.g batteries or hydrogen storage capacity. A typical turndown ratio of a fuel system is about 1:5 and high efficiencies are kept to at least 50% load.

3. Fuel cells have a potential for high reliability as the number of moving parts is low. It consists of auxiliary equipment such as fans and pumps. The target for life length of fuel cells is usually given as 40000 h for the stack and at least twice the number of hours for the system. This target has been reached for a small number of fuel cells but in general it still remains to be proven.

3.1.2 Advantages of Fuel Cells

The primary benefits of fuel cells are the potential for increased system efficiency and reduced greenhouse gas emissions; also the fuel flexibility is one of the important benefits of fuel cells. Another advantage is the possibility of cogeneration which means producing heat in addition

to the electrical energy. Some other benefits are modularity, simplicity of installation, silent operation, and suitability for the integration with renewable energy sources.

3.1.3 Disadvantages of Fuel Cells

The main drawback s their extremely high cost, also, more effort and research are required to demonstrate endurance and reliability of high temperature units.

3.2 Fuel Cell Workings

The workings of the fuel cells are based on fundamental electrochemical principles [29]. The reaction of hydrogen gas (H_2) and oxygen gas (O_2), to form water, is the form of reaction in the process as presented in [30]:

$$2H_2 + O_2 \Rightarrow 2H_2O \tag{3.1}$$

The fuel cells have an electrolyte between two electrodes. The process occurs naturally and is caused by the fact that charged particles migrate towards regions of lower electrochemical energy.

The charged particles of hydrogen and oxygen migrate towards each other and connect together since the final products have lower electrochemical energy [30]. It is essential to separate electrons from protons and to regulate the movement of the electrons. This can be accomplished by separating the hydrogen and oxygen by an electrolyte, which completely insulates electrons and allows protons from the hydrogen atoms to move through. An external path is formed from electrons using an electrical load to generate useful electrical energy [30] as shown in Figure 3.2.

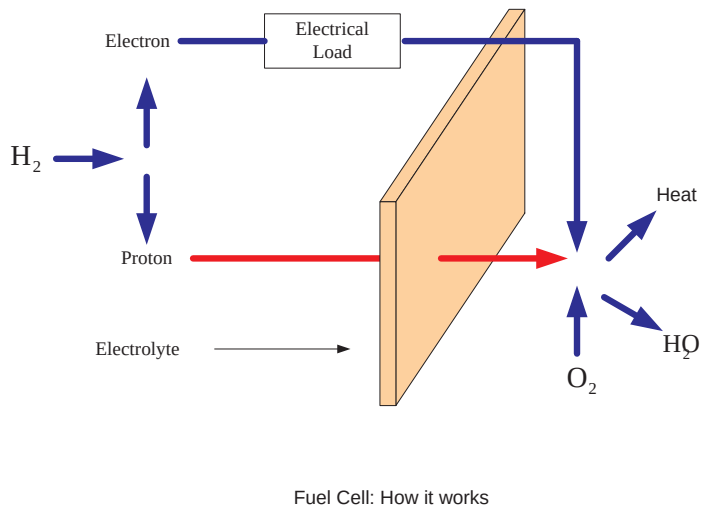

Figure 3.2: Fuel cell. principles of operation.

3.3 Modelling of SOFC

Solid Oxide Fuel Cells (SOFC) are particularly attractive because they are the most efficient in terms of fuel input to electricity output. The technology is best applicable in the MG. The high operating temperature produces heat suited well to cogeneration applications. SOFC do not contain noble metals and do not utilize liquid electrolytes which can cause problems and be expensive [31].

The stack model will be based on the following assumptions:

1. The gases are ideal.
2. The stack is fed with hydrogen and air. If natural gas instead of hydrogen is used as fuel, the dynamics of the fuel processor must be included in the model, upstream of the hydrogen inlet, as a first order transfer function [32]. The transfer function gain should reflect the changes in composition occurring during the process. The effect of the fuel processor in the model will be tested in the future.
3. The channels that transport gases along the electrodes have a fixed volume, but their lengths are small, so that it is only necessary to define one single pressure value in their interior.
4. The exhaust of each channel is via a single orifice. The ratio of pressures between the interior and exterior of the channel is large enough to consider that the orifice is choked.
5. The temperature is stable at all times.
6. The only source of losses is ohmic, as the working conditions of interest are not close to the upper and lower extremes of current.
7. The Nernst's equation can be applied.

The change in concentration of each species that appears in the SOFC chemical reactions can be written generally in terms of input and output flows into a control volume as well as net generation due to the material balance equation:

$$(\frac{P_r Vo}{R_{gass} T})\dot{x} = N_i^{in} - N_i^0 + N_i^r \tag{3.2}$$

where Vo is the cell volume, N_i^{in} ,N_i^0 are the flow rates (mole/s) of the ith reactant at the cell input and output (exit), respectively, N_i^r is the reaction rate (mole/s) of the ith reactant. P_r is the cell pressure (atm), T is the cell temperature in ^oK , and R_{gass} is the gas constant (8.31 J/mole ^oK).

3.3.1 Characterization of the exhaust of the channels

According to [33], an orifice that can be considered choked, when fed with a mixture of gases of average molar mass M [kg/kmol] and similar specific heat ratios, at a constant temperature, assumes the following form:

$$\frac{W}{P_r u} = K\sqrt{M} \tag{3.3}$$

where, W is the mass flow [kg/s], K is the valve constant, mainly depending on the area of the orifice $\left[\frac{\sqrt{kmol.Kg}}{atm.s}\right]$, and P_ru is the pressure upstream (inside the channel) [atm].

For the anode, the concept of fuel utilization U_f can be introduced, as the ratio between the fuel flow that reacts and the fuel flow injected to the stack. U_f is also a way to express the water molar fraction at the exhaust. According to this definition, equation (3.3) can be written as:

$$\frac{W_{an}}{P_{an}} = K_{an}\sqrt{(1-U_f)M_{H_2} + U_f M_{H_2O}} \tag{3.4}$$

where W_{an} is the mass flow through the anode valve [kg/s], K_{an} is the anode valve constant, $\left[\frac{\sqrt{kmol.Kg}}{atm.s}\right]$, M_{H_2}, M_{H_2O} are the molecular masses of hydrogen and water, respectively [kg/kmol], and P_{an} is the pressure inside the anode channel [atm].

Assuming that the molar flow of any gas through the valve is proportional to its partial pressure inside the channel, then according to [33]:

$$\frac{q_{H_2}}{P_{H_2}} = \frac{K_{an}}{\sqrt{M_{H_2}}} = K_{H_2} \tag{3.5}$$

$$\frac{q_{H_2O}}{P_{H_2O}} = \frac{K_{an}}{\sqrt{M_{H_2O}}} = K_{H_2O} \tag{3.6}$$

where

q_{H_2O} ,q_{H_2} are the molar flows of water and hydrogen, respectively, through the anode valve [kmol/s]. P_{H_2O},P_{H_2} are the partial pressures of water and hydrogen, respectively [atm]. K_{H_2O}, K_{H_2} are the valve molar constants for water and hydrogen, respectively $[\frac{kmol}{s.atm}]$.

[33] introduces the following expression:

$$\frac{W}{P_{an}} = K_{an}.\left[(1-U_f)\sqrt{M_{H_2}} + U_f\sqrt{M_{H_2O}}\right] \tag{3.7}$$

Comparison of (3.4) and (3.7) indicates that for $U_f > 70\%$ the error is less than 7%. It is possible to redefine slightly (3.5) and (3.6) so that it is even lower. The same study for the cathode shows that the error in that valve is even lower, because of the similar molecular masses of oxygen and nitrogen.

3.3.2 Calculation of the partial pressures

Every individual gas will be considered separately, and the perfect gas equation will be applied to it. We will take the hydrogen as an example:

$$P_{H_2}V_{an} = n_{H_2}R_{gass}T \tag{3.8}$$

where V_{an} is the volume of the anode,n_{H_2} is the number of hydrogen moles in the anode channel, R is the universal gas constant $[\frac{l.atm}{kmol.K}]$, T is the absolute temperature $[K]$.

By isolating the pressure and taking the derivative of the previous equation, we can write:

$$\frac{d}{dt}P_{H_2} = \frac{R_{gass}T}{V_{an}}q_{H_2} \tag{3.9}$$

where, q_{H_2} is the time derivative of n_{H_2}, and represents the hydrogen molar flow q_{H_2} [kmol/s].

There are three relevant contributions to the hydrogen molar flow q_{H_2}: the input flow $q_{H_2}^{in}$, the flow that takes part in the reaction $q_{H_2}^{r}$ and the output flow $q_{H_2}^{out}$ [33],[34]. Therefore (3.9) can be expressed as:

$$\frac{d}{dt}P_{H_2} = \frac{R_{gass}T}{V_{an}}(q_{H_2}^{in} - q_{H_2}^{out} - q_{H_2}^{r}) \tag{3.10}$$

The molar flow of hydrogen that reacts $q_{H_2}^{r}$ can be calculated according to the basic electrochemical relationship as:

$$q_{H_2}^{r} = \frac{N_0 I}{2F} = 2K_r I^r \tag{3.11}$$

where N_0 is the number of cells associated in series in the stack, F is the Faraday's constant [C/kmol], I^r is the stack current [A], and K_r is a constant defined for modelling purposes [$\frac{kmol}{s.A}$].

Substituting equation (3.11) into (3.10):

$$\frac{d}{dt}P_{H_2} = \frac{R_{gass}T}{V_{an}}(q_{H_2}^{in} - q_{H_2}^{out} - 2K_r I^r) \tag{3.12}$$

Substituting the output flow of equation (3.5) into (3.12), taking Laplace transform of both sides, and solving for the hydrogen partial pressure results in:

$$sP_{H_2} = \frac{R_{gass}T}{V_{an}}(q_{H_2}^{in} - K_{H_2}P_{H_2} - 2K_r I^r) \tag{3.13}$$

and after some algebraic manipulation in (3.13)

$$P_{H_2} = \frac{1/K_{H_2}}{1 + s\tau_{H_2}}(q_{H_2}^{in} - 2K_r I^r) \tag{3.14}$$

where τ_{H_2}, expressed in seconds, is the time constant of the system associated with the hydrogen flow. It is a function of temperature and has the form:

$$\tau_{H_2} = \frac{V_{an}}{K_{H_2}R_{gass}T} \tag{3.15}$$

For calculating the stack voltage we apply Nernst's equation and Ohm's law (to consider ohmic losses). The stack output voltage V^r can be represented by the following expression:

$$V^r = N_0\left(E_0 + \frac{R_{gass}T}{2F}\left[\ln\frac{P_{H_2}P_{O_2}^{0.5}}{P_{H_2O}}\right]\right) - rI^r \tag{3.16}$$

where

E_0 is the voltage associated with the reaction free energy [V]. R is the same gas constant as previously, but care should be taken with the system unit [$\frac{J}{kmol.K}$] [33].

r describes the ohmic losses of the stack [Ω].

The above equations provided by [33] from the basic SOFC power section dynamic model used for performance analysis during normal operation. In [35] the SOFC power generation was modelled by adding control strategy of the fuel cell system, models of fuel processor, and the power section:

(1) Although CO can be a fuel in SOFC, the CO-shift reaction is chemically favored with present designs and operations if the fuel gas contains water. The CO-shift reaction is:

$$\mathrm{CO} + \mathrm{H_2O} \rightarrow \mathrm{CO_2} + \mathrm{H_2} \tag{3.17}$$

Based on this, it is assumed that only $\mathrm{H_2}$ and $\mathrm{O_2}$ enter into the fuel cells.

(2) Fuel utilization is the ratio between the fuel flow that reacts and the input fuel flow. Hence, we have

$$U_f = {}^{\mathrm{r}}q_{\mathrm{H_2}}/_{\mathrm{q}}{}^{in}_{\mathrm{H_2}} \tag{3.18}$$

As in equation (3.11) an $80 - 90\%$ fuel utilization is used and the demand current can be restricted to the range:

$$\frac{0.8q^{\mathrm{in}}_{\mathrm{H_2}}}{2K_r} \leq I^{in} \leq \frac{0.9q^{\mathrm{in}}_{\mathrm{H_2}}}{2K_r} \tag{3.19}$$

(3) The real output current in the fuel cell system can be measured, so the input fuel flow can be controlled to control U_f to be 85%, so:

$$q^{\mathrm{in}}_{\mathrm{H_2}} = \frac{2K_rI^r}{0.85} \tag{3.20}$$

(4) From the overall fuel cell reaction (3.1), the stoichiometric ratio of hydrogen to oxygen is 2 to 1. Oxygen excess is always taken in to let hydrogen react with oxygen more completely. Their simulation in fuel cell system shows that r_{H-O} should be kept around 1.145 in order to keep the fuel cell pressure difference below 4 kPa under normal operation. So the input oxygen flow is controlled to keep r_{H-O} at 1.145 by speed control of the air compressor.

(5) The peak power capacity is the ratio of maximum theoretical power delivery to the rated power in the fuel cell system. It is only determined with the available active fuel cell area. For the highest possible total efficiency and the dynamic load-following behavior, p_k should be as large as possible. As this value is directly proportional to the effective fuel cell area for a constant output, cost considerations restrict the upper value to be between 130 and 180% . In practice, this upper value is also restricted by the safety of system operation. In order to prevent damage to the electrolyte, the fuel cell pressure difference between the hydrogen and oxygen passing through the anode and cathode gas compartments should be below 4 kPa under normal operation and 8 kPa under transient conditions. Because different fuel cell systems have different peak power capacity, simulation shows that p_k in the fuel cell system model should be below 170%, which means the maximum power delivery of the fuel cell system is below 1.7 times of the rated power.

(6)The chemical reaction is modeled as a first-order transfer function with a 5 s time constant because of the fuel processor is usually slow as it is associated with the time to change the chemical reaction parameters after a change in flow reactions.

(7) The electrical response time in the fuel cells is generally fast and mainly associated with the speed at which the chemical reaction is capable of restoring the charge that has been drained by the load. This is also modeled as a first-order transfer function but with a 0.8 s time constant.

(8) The fuel cell system can output not only real power but also reactive power. This is done at the power conditioner (it converts DC power to AC power and includes current, voltage

and frequency control). Usually, power factor (PF) can be in the range of 0.8 to 1. Because the response time of the power conditioner is less than 10 ms, it is concluded that it is not necessary to include its detailed model in the slow dynamic fuel cell system. It is assumed that PF can be adjusted accordingly by the power conditioner.

Based on [33] and the above discussions, the SOFC system dynamic model which is proposed by [35] is summarized in (3.21)-(3.25). The block diagram of the system is given in Figure 3.3.

$$\begin{array}{l} \frac{dI^r}{dt} = \frac{1}{T_e}\left[-I^r + I_{ref}\right] \\ \frac{dq_{H_2}^{in}}{dt} = \frac{1}{T_f}\left[-q_{H_2}^{in} + \frac{2K_r}{U_{opt}} I^r\right] \\ \frac{dP_{H_2}}{dt} = \frac{1}{\tau_{H_2}}\left[-P_{H_2} + \frac{1}{K_{H_2}}\left[q_{H_2}^{in} - 2K_r I^r\right]\right] \\ \frac{dP_{H_2O}}{dt} = \frac{1}{\tau_{H_2O}}\left[-P_{H_2O} + \frac{2K_r}{K_{H_2O}} I^r\right] \\ \frac{dP_{O_2}}{dt} = \frac{1}{\tau_{O_2}}\left[-P_{O_2} + \frac{1}{K_{O_2}}\left[\frac{1}{r_{HO}} q_{H_2}^{in} - K_r I^r\right]\right] \end{array} \tag{3.21}$$

$$I_{ref} = \begin{cases} q_{H_2}^{in}\frac{U_{\max}}{2K_r}, & \text{if} \quad \tilde{I} > q_{H_2}^{in}\frac{U_{\max}}{2K_r} \\ q_{H_2}^{in}\frac{U_{\min}}{2K_r}, & \text{if} \quad \tilde{I} < q_{H_2}^{in}\frac{U_{\min}}{2K_r} \\ \tilde{I} = P_{ref}/V^{in}, & otherwise \end{cases} \tag{3.22}$$

$$\tilde{I} = \frac{1}{V_{in}}(P_{ref} - \Delta P) \tag{3.23}$$

$$V^r = N_0\left(E_0 + \frac{R_{gass}T}{2F}\left[\ln\frac{P_{H_2}P_{O_2}^{0.5}}{P_{H_2O}}\right]\right) - rI^r \tag{3.24}$$

The active (DC) power produced by the fuel cell is then given by the following relation:

$$P_e = V^r I^r \tag{3.25}$$

where I^r is the fuel cell stack current; V^r is the DC voltage across the stack of the fuel cells is governed by the Nernst equation, $q_{H_2}^{in}$ stands for the hydrogen input flow; and P_{H_2}, P_{O_2} , P_{H_2O} denote the partial pressures of hydrogen, oxygen, and water, respectively. The time constants T_e, T_f , τ_{H_2} , τ_{H_2O}, τ_{O_2} , designate the electrical response time of the fuel cell, fuel processor response time, response times of hydrogen, water, and oxygen flows, respectively. K_{H_2} , K_{H_2O}, and K_{O_2} , denote the valve molar constants for hydrogen, water, and oxygen. The auxiliary constants $Uopt$, $U_{\max}$, and $U_{\min}$ stand for the optimal, maximum, and minimum fuel utilization, respectively. Finally, $K_r = N_0/(4F)$. The numerical values of the aforementioned constants can be found in [33] and [35].

3.4 Simulation Results

In this work we assume that the SOFC fuel system is a stand-alone system and is operating with a constant rated voltage 1.0 p.u. and power demand 0.7 p.u. The other parameters are the same as in [35].

Figure 3.4 shows a dynamic step response of a SOFC fuel cell system. From the simulation result, we can notice that the output power started to increase after 2 to 3 seconds. The step

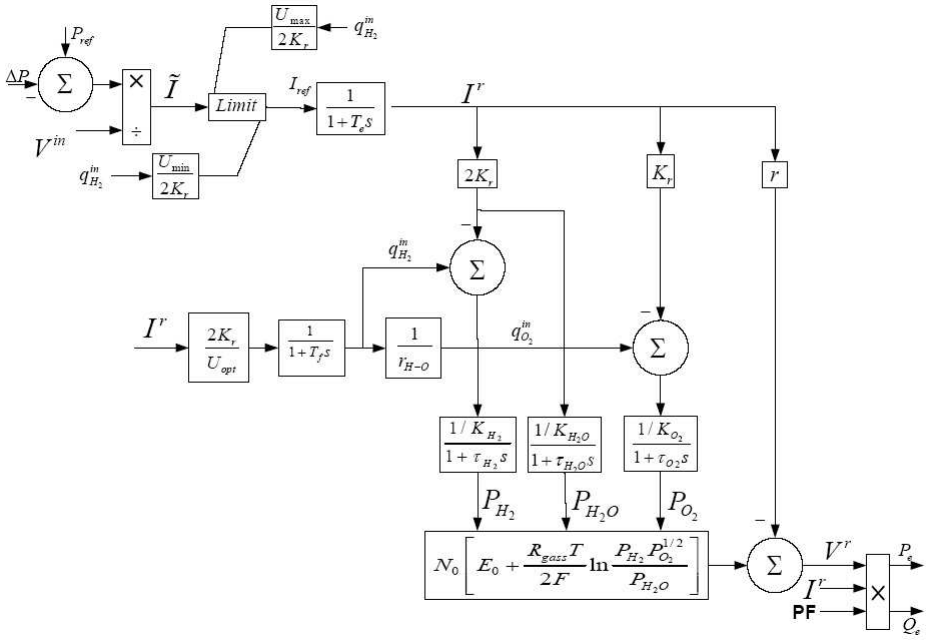

Figure 3.3: SOFC system dynamic model.

increase of the demand power is related to the fast electrical response of the fuel cell. After that, the output power started to increase slowly until it reached the demand power. This is due to the slow chemical response time of the fuel processor.

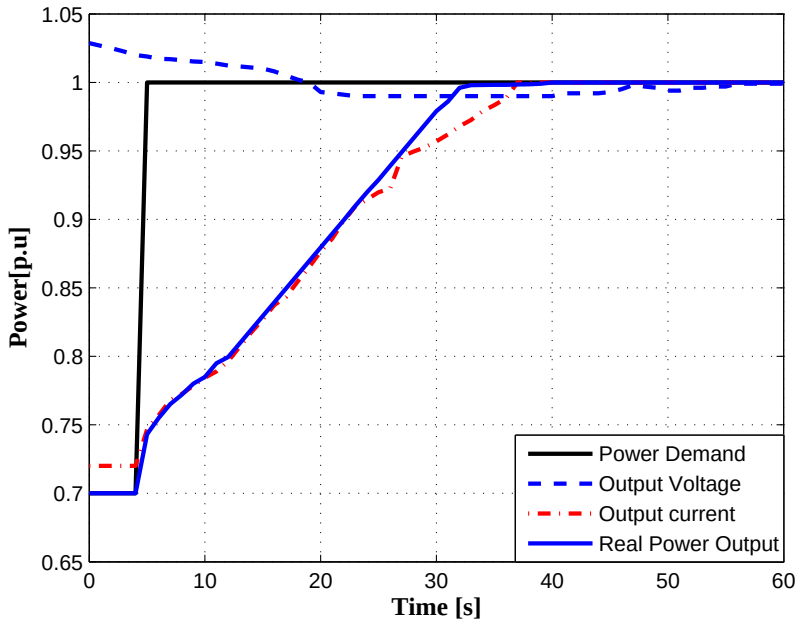

Figure 3.4: Responses output voltage, output current, real power output due to the power demand input.

Figure 3.5 illustrates the response of the fuel cell pressure difference between hydrogen and oxygen. We can notice that it increases to the peak value of 3.5 kPa, which is less than the maximum safety pressure difference 8 kPa. It can return to the normal operating pressure difference value around 0 kPa.

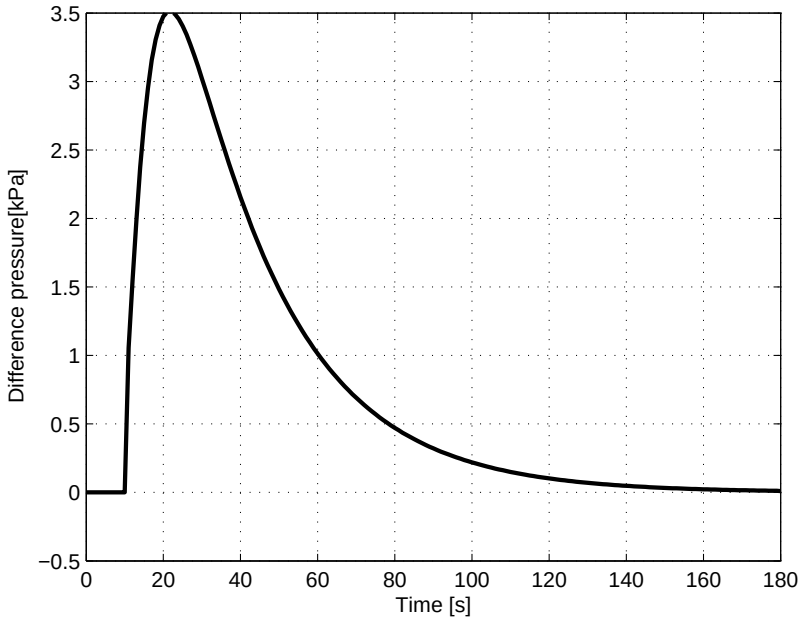

Figure 3.5: Response of pressure difference between hydrogen and oxygen.

In Figure 3.6 the fuel utilization response is presented, due to increase in the power demand, the fuel utilization increases to the maximum fuel utilization $U_{\max}$ in about 5 s. After staying at $U_{\max}$ for about 25 s, it decreases to optimal fuel utilization U_{opt}.

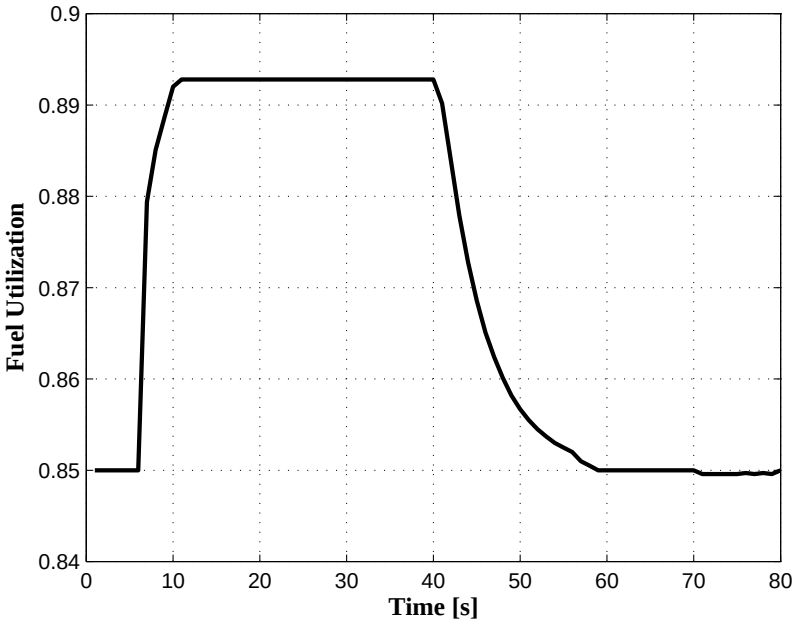

Figure 3.6: Response of Fuel Utilization.

Chapter 4

Micro Turbines

4.1 Overview of Micro-Turbines

Micro turbines (MTs) are small high-speed gas turbines powered generators ranging in size from 25 to 500kW [36]. The operation principle of the MTs follows the same principles of conventional gas turbine depending on Brayton (constant pressure) cycle [36], [37]. Small gas turbine engines were initially developed by Alison in the 1960s for ground transportation [37]. The micro-turbine provides input mechanical energy for the MT generator system, which is converted by the generator to electrical energy. The generator nominal frequency is in the range of 1.4-4 kHz. This frequency is transformed to the desired power frequency of 50/60 Hz by a converter. The electrical energy, passing through the transformer, is delivered to the distribution system and the local load. The transformer boosts the converter output voltage up to the voltage level of the distribution system. The components of the MT generator system are described in detail in the subsections following [38].

4.2 Construction of Micro-Turbines

The components of a MT are shown in Figure 4.1. The main components include a gas turbine and recuperator, electrical system, an exhaust gas heat exchanger, supervision and control system, and a gas compressor. As can be seen, an extra heat exchanger is used to heat water with the hot exhaust gases coming out the recuperator. Filtered air at atmospheric pressure and temperature is pressurized in the compressor before entering the combustor. A controlled amount of injected fuel is mixed with the compressed air in the combustor and the mixture is ignited. The combustion products at high temperature and pressure flow and expand over the turbine blades to produce mechanical energy. Most constructions of MTs depend on a single shaft designed to rotate at a high speed in the range of 50krpm to 120krpm [37]. Thus, a high speed Permanent Magnet Synchronous Generator (PMSG) is used to produce variable voltage AC power at high angular frequencies up to 1000 rad/s. A part of the extracted horsepower in the turbine is used for driving the air compressor. The recuperator is used to improve the overall efficiency of the system by transferring the waste heat from the exhaust gas to the combustion air stream. The high frequency of the generated power can be reduced using cycloconverters or rectifier- inverter system.

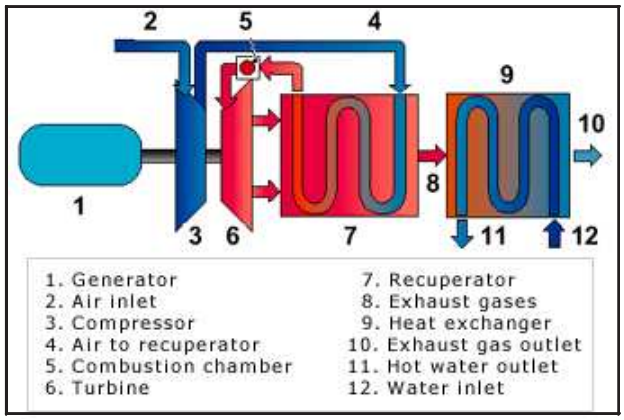

Figure 4.1: Principle components of micro turbine unit.

4.3 Major features of Micro- Turbines

The newly developed MTs have the following advantages [37]:

- Easy installation and infrastructure requirements (install the units almost anywhere- on a pole, platform, in a substation, roof, vault or pad).
- Low maintenance cost - less than \$0.005/kWH.
- Multi- fuel capability (diesel, gasoline, ethanol, propane).
- Reliable and durable due to the simplicity of the structure
- Environmental superiority of MTs on natural gas.
- High efficiency, with fuel energy-to- electricity conversion reaching $25\% - 30\%$.
- Possibility of cogeneration by using the waste heat recovery, which could achieve overall energy efficiency levels reaching 75%.

4.4 Application of Micro-Turbines

The following application examples will be provided with insight, to the low cost, high efficient MTs [37]:

- Firm power for isolated communities, small commercial buildings and light industry.
- Peak shaving for utility systems in order to decrease the required incremental cost to serve additional loads.
- Standby and emergency power for more reliable operation of the utility and with important loads.
- Uninterruptible power supply (UPS) since they provide low initial cost, low maintenance requirements and high reliability.

Because large steam turbines and large synchronous generators have dominated power generation, the steady state and dynamic behaviour for these systems is well understood. The basic operation and control principles are summarized below [39]:

- At steady state, the power of the steam rate into the turbine is equal to the electrical power removed from the generator. The speed of the generator and turbine is considered to be synchronous, implying that output electrical sinusoids are in phase with the grid. This operation requires good speed control of the turbine.

- During a load transient, the change in power is taken from the speed of the rotor of the large turbine and generator. Because these devices are enormous, there is considerable stored energy in the rotating masses. The speed control of the turbines sees this speed change and corrects the rate at which the steam is supplied to the turbine, correcting the speed until the set point is achieved. In this manner, the turbine generator set is capable of nearly instantaneous load tracking.

The same base of knowledge is not available for micro-turbines and generators. However, the same basic principles apply and are summarized below.

- At steady state, the power of the natural gas combustion and air into the turbine is equal to the electrical power removed from the generator. The speed of the generator and turbine is not critical, as the output sinusoids from the generator are rectified. The dc link voltage needs to be supported to ensure that conservation of power requirements are met. This operation requires good speed control of the turbine.

- During a load transient, the change in power is taken from the speed of the rotor of the micro-turbine. However, because these devices are small, there is very little stored energy in the rotating masses and the speed of the rotor changes very quickly. The speed control of the micro-turbines sees this speed change and corrects the rate at which the fuel is supplied to the micro-turbine, correcting the speed until the set point is achieved. The speed of micro-turbine needs to be changed quickly to ensure that the generator does not stall. In this manner, the turbine generator set is capable of load tracking.

4.5 Micro-Turbine Modelling

The micro turbine is a high frequency AC source the output of which need to be rectified. The DC voltage needs to be interfaced to the network using a voltage source inverter. The slow response requires either a DC bus or a AC system storage to insure load tracking. Figure 4.2 illustrates the outline of a micro turbine. The micro turbine requires a power electronic circuit for interfacing with the AC load. This interface consists of an AC to DC rectifier, a DC bus with capacitor and a DC to AC inverter.

Figure 4.3 shows the equivalent circuit of the generator and the rectifier which can be modelled as a 3-phase, full wave, diode bridge rectifier with the AC source which is assumed to be a permanent magnet generator.

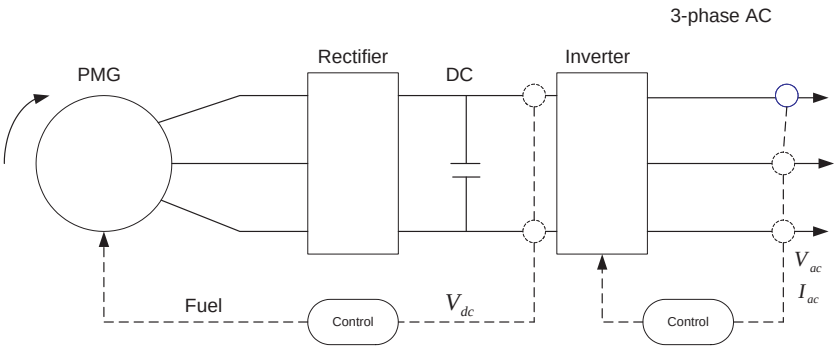

Figure 4.2: Outline of a micro turbine generator.

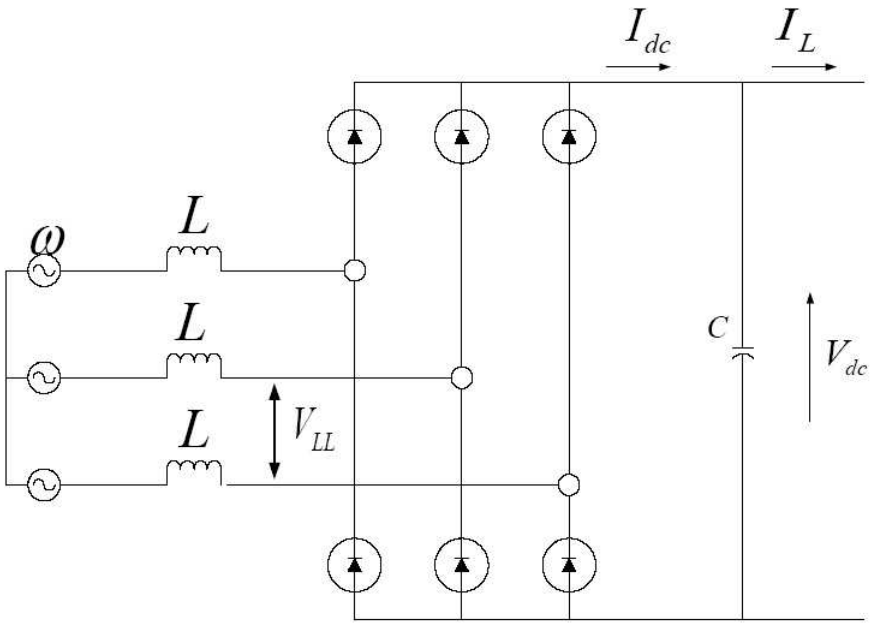

Figure 4.3: The equivalent circuit.

No load case is considered (Ideal). The voltage induced on the generator terminal V_{LL} can be expressed as:

$$V_{LL} = K_v \omega \sin(\omega t) \tag{4.1}$$

$$V_{LL} = K_v \omega \mathrm{Im}\left\{e^{j\omega t}\right\} \tag{4.2}$$

where K_v is the voltage constant and ω is the electrical angular frequency. The output DC voltage is given by:

$$V_{dc} = \frac{3}{\pi} |V_{LL}| - \frac{3\omega L}{\pi} I_{dc} \tag{4.3}$$

Substituting (4.1) into (4.3) we have:

$$V_{dc} = \frac{3}{\pi} K_v \omega - \frac{3}{\pi} \omega L . I_{dc} \tag{4.4}$$

This can be written as:

$$\frac{3}{\pi}K_v\omega = V_{dc} + \frac{3}{\pi}\omega L.I_{dc} \tag{4.5}$$

Define the no load DC voltage E_g by:

$$E_g = K_e\omega = \frac{3K_v}{\pi}\omega \tag{4.6}$$

where $K_e = \frac{3K_v}{\pi}\ \{V/(rad/\sec)\}$
Then (4.5) can be expressed as:

$$E_g = V_{dc} + K_x.\omega.I_{dc} \tag{4.7}$$

where $K_x = \frac{3L}{\pi}\ \{\Omega/(rad/\sec)\}$

Equation (4.5) describes the electromechanical nature of the system. Therefore if the system has no losses, the input power P_m can be expressed as a function of I_{dc} :

$$P_m = V_{dc}I_{dc} \tag{4.8}$$

Using equation (4.6) and (4.7) this becomes .

$$P_m = K_e\omega I_{dc} - K_x\omega I_{dc}^2 \tag{4.9}$$

The mechanical shaft torque for the no loss system T_m is expressed as equation (4.10) :

$$T_m = \frac{P_m}{\omega} = K_eI_{dc} - K_xI_{dc}^2 \tag{4.10}$$

The mechanical part of the system is represented by:

$$\frac{d\omega}{dt} = \frac{1}{J_r}(T_m - T_t) \tag{4.11}$$

where J_r is the inertia of the shaft, T_m is the mechanical torque, T_t is the load torque.
Additionally, the DC voltage V_{dc} can also be expressed as:

$$V_{dc} = \frac{1}{C}\int (I_{dc} - I_L)dt \tag{4.12}$$

The relations in equations (4.4) and (4.12) determine the load current I_L and the final output power. Finally from all of the above equations the block diagram of an MT generator model is described in Figure 4.4:

4.6 Inverter Model

Inverters are used both for feeding power from distributed generators to the transmission grid, and for draining power to various types of electronic loads. Micro Turbine systems and Fuel Cells need to be connected to the grid via inverters, which are used to convert DC power to AC power as shown in Figure 4.5. The over all system contains three basic elements: a micro-source, a DC interface and a voltage source inverter.

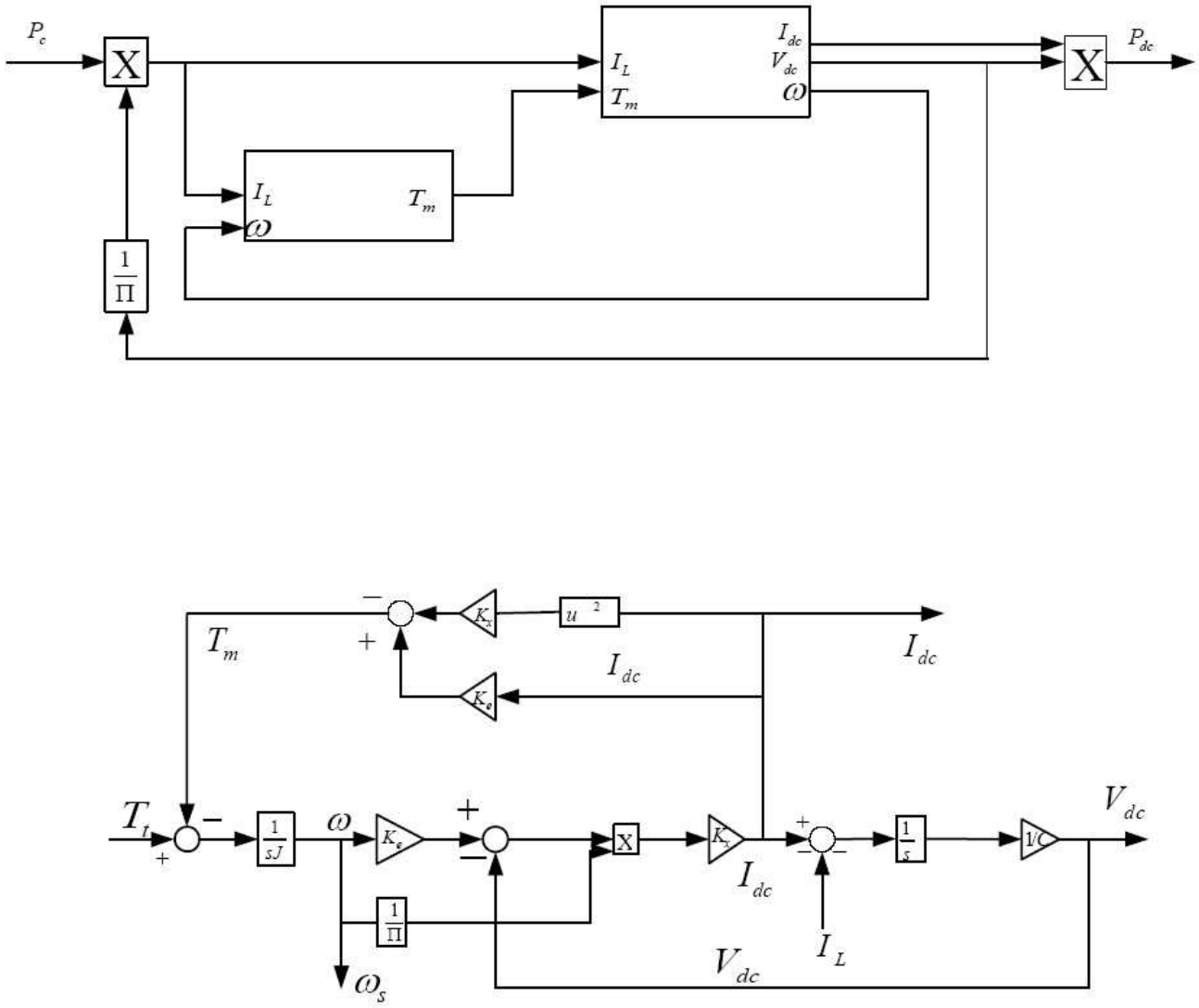

Figure 4.4: The micro turbine generator model.

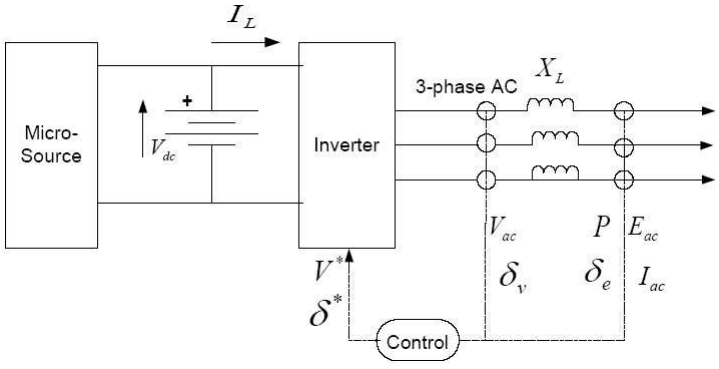

Figure 4.5: Interface Inverter System

The DC voltage is denoted by V_{dc}, V_{ac} corresponds to AC voltage, V^* represents the output voltage from the control unit. Coupling to the power system is done through connection reactance X_L. The voltage source inverter provides control of both the magnitude and phase of its

output voltage, V_{ac}. The vector relationship between the inverter voltage, V_{ac}, and the system voltage, E_{ac}, along with the connection reactance, X_L, determines the flow of real and reactive power (P,Q) from the microgrid to the system [5], [39].

As a minimum the inverters needs to control the flow of real power P , and reactive power Q between the micro sources and the power system. The P and Q are coupled. For small changes, P is predominantly dependent on the power angle, δ_P, while Q depends on voltage difference. The power flow equations are:

$$P = \frac{VE_{ac}}{X_L} \sin \delta_P \tag{4.13}$$

$$Q = \frac{V}{X_L}(V - E_{ac} \cos \delta_P) \tag{4.14}$$

The power angle δ_P is:

$$\delta_P = \delta_V - \delta_e \tag{4.15}$$

where δ_V is corresponds to inverter terminal voltage phase angel, δ_e denotes grid voltage phase angle.

In the range of small $\delta_e, \sin(\delta_e) \approx \delta_e$ holds and the relationship between P and δ_e can be regarded as almost linear [5]. By using these characteristics, inverters are controlled by power width modulation (PWM) to get the required values of P and Q. However in this thesis inverters are modeled by means of ideal voltage sources, which achieve the same behavior, as simplified models.

Figure 4.6 shows the details of a droop governor [40]. This governor has two important characteristics. First, it allows maintaining any desired value of power when the AC grid is connected. Second, it slowly brings up the frequency near the customary ω_0 value after the droop regulation has taken place.

The constant m in Figure 4.6 denotes the frequency droop without the frequency restoration loop active. It is dependent on the local power setpoint before islanding, and the new power setpoint to be reached after the grid has failed. k', k'' are gains dependent on the power setpoint.

The equation that allows the droop to work is:

$$\omega^*(t) = \omega_0 - m(P_c - P(t)) \tag{4.16}$$

From the integral block of Figure 4.6:

$$\frac{dP_c}{dt} = k''[(\omega_0 - \omega_i) + k'(P^* - P_c)] \tag{4.17}$$

The PI is a block with a proportional and integral gain as indicated below: $K_p + \frac{K_i}{s}$

Based on [5] the microturbine model is summarized in (4.18)-(4.28). The block diagram of the system is given in Figure 4.4

$$V_{LL} = K_v \omega \sin(\omega t) \tag{4.18}$$

$$V_{dc} = \frac{3}{\pi} |V_{LL}| - \frac{3\omega L}{\pi} I_{dc} \tag{4.19}$$

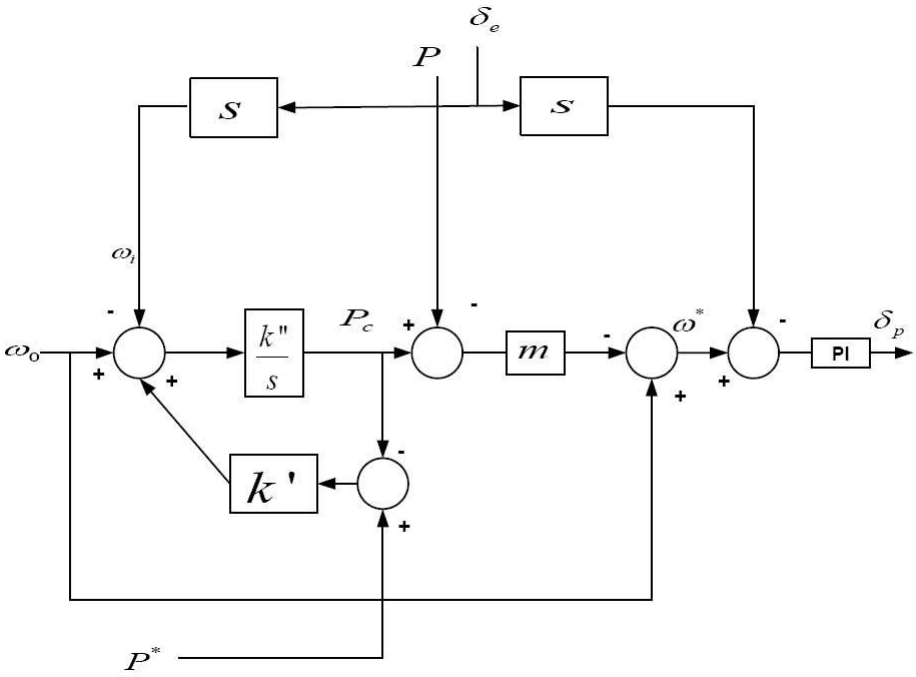

Figure 4.6: Power with frequency droop.

$$V_{dc} = \frac{3}{\pi} K_v \omega - \frac{3}{\pi} \omega L . I_{dc} \tag{4.20}$$

$$\frac{3}{\pi} K_v \omega = V_{dc} + \frac{3}{\pi} \omega L . I_{dc} \tag{4.21}$$

$$E_g = K_e \omega = \frac{3K_v}{\pi} \omega \tag{4.22}$$

where $K_e = \frac{3K_v}{\pi}$ $\{V/(rad/\sec)\}$

$$E_g = V_{dc} + K_x . \omega . I_{dc} \tag{4.23}$$

where $K_x = \frac{3L}{\pi}$ $\{\Omega/(rad/\sec)\}$

$$P_m = V_{dc} I_{dc} \tag{4.24}$$

$$P_m = K_e \omega I_{dc} - K_x \omega I_{dc}^2 \tag{4.25}$$

$$T_m = \frac{P_m}{\omega} = K_e I_{dc} - K_x I_{dc}^2 \tag{4.26}$$

$$\frac{d\omega}{dt} = \frac{1}{J}(T_m - T_t) \tag{4.27}$$

$$V_{dc} = \frac{1}{C} \int (I_{dc} - I_L) dt \tag{4.28}$$

4.7 Simulation Results

The turbine generator tested in simulations was a 75-kW Parallon micro-turbine made by Honeywell[41]. The power reference signal consists of negative power steps of 15 kW lasting 30 s starting from 75 kW, stepping down to 0 kW and then stepping back up to 75 kW, as presented in Figure 4.7:

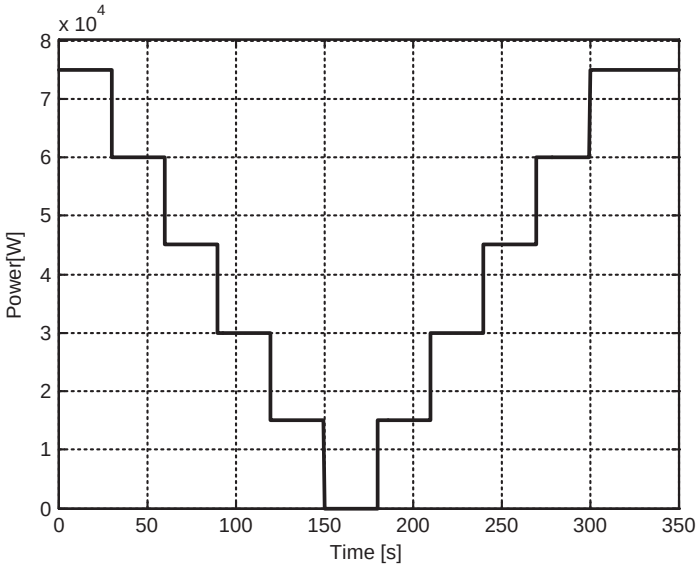

Figure 4.7: Power command to the microturbine system

The microturbine system response to this power command is displayed in Figures 4.8- 4.11. Figure 4.8 shows the output power of the system; Figure 4.9 the shaft speed; Figure 4.10 the DC link voltage; and Figure 4.11 the rotor speed.

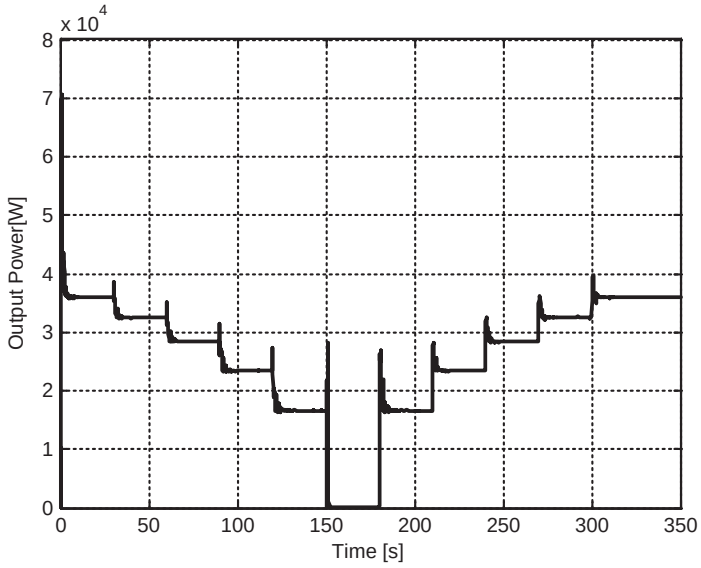

Figure 4.8: The output power of the microturbine P

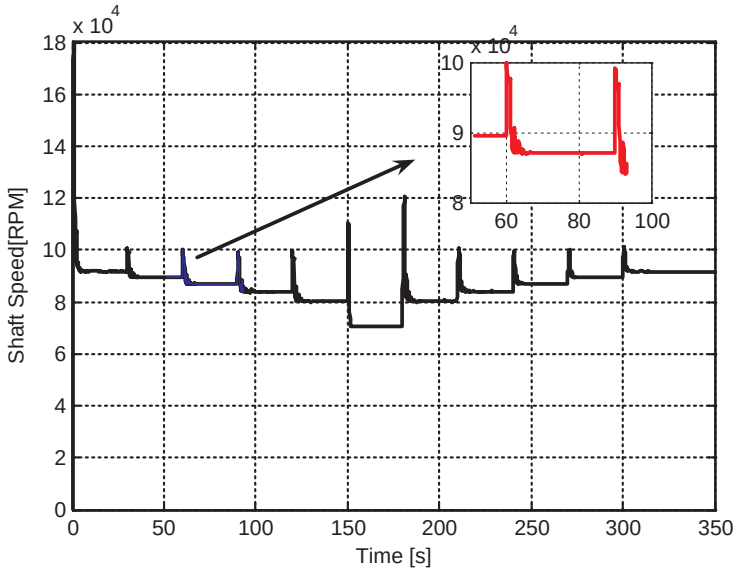

Figure 4.9: Shaft speed of the microturbine model ω

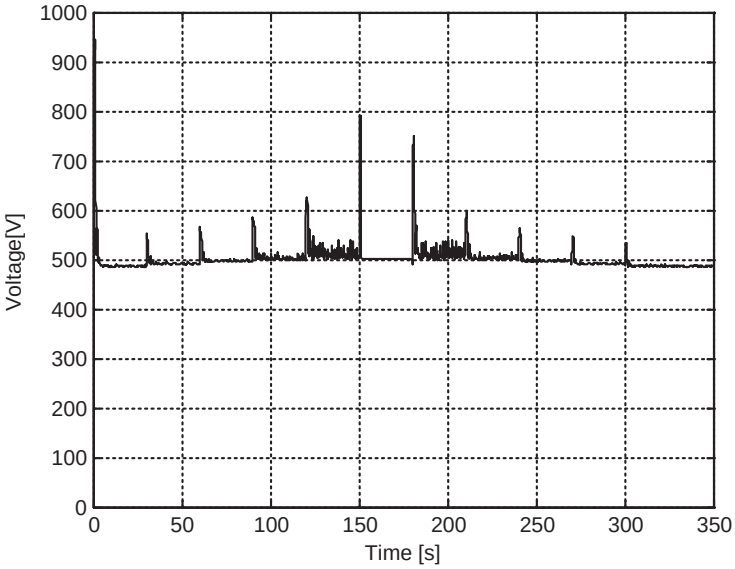

Figure 4.10: DC link Voltage of the microturbine model V_{DC}

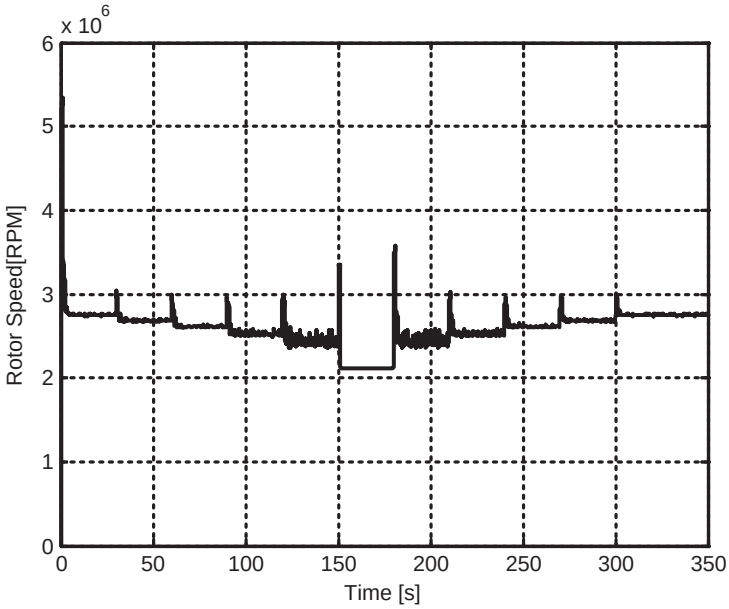

Figure 4.11: Rotor Speed of the microturbine model

However, there are some responses which do not follow the reference trajectories, such as the rotor speed at higher power levels and the dc link voltage steady state value for mid-level output power. It is believed that a better tuned controller, would result in improved results. More complex controllers could also be added to improve the response.

Chapter 5

Wind Turbine

5.1 Introduction

Wind energy is expected to be one of the most prominent sources of electrical energy in years to come. The increasing concerns of environmental issues demand the search for more sustainable electrical sources. Wind turbines along with solar energy and fuel cells are possible solutions for the environmental-friendly energy production. In this theses, the wind power as integrated system will be studied.

Wind turbines are packaged systems that include a rotor, a generator, turbine blades, and a drive or a coupling device. As wind blows through the blades, the air exerts aerodynamic forces that cause the blades to turn the rotor. As the rotor turns, its speed is altered to match the operating speed of the generator. Most systems have a gearbox and a generator in a single unit behind the turbine blades. As with photovoltaic (PV) systems, the output of the generator is processed by an inverter that changes the electricity from DC to AC so that the electricity can be used.

5.2 Wind Turbine Generating System

The working principles of the wind turbine can be described in two processes, that are carried out by its main components: the rotor which extracts kinetic energy from the wind passing it and converts it into mechanical torque and the generating system, the job of which is to convert this torque into electricity. Figure 5.1 illustrates the working principles of a wind turbine.

Basically, a wind turbine can be equipped with any type of a three phase generator. Several generations types may be used in wind turbines [42], but here we will discuss three types of wind turbine generators:

- Squirrel cage induction generators.
- Doubly fed (wound rotor) induction generators.
- Direct drive synchronous generators.

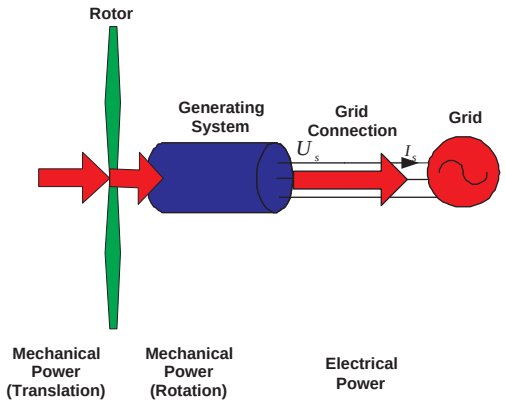

Figure 5.1: General working principle of wind power generation.

5.2.1 Squirrel Cage Induction Generator

It is the oldest and the simplest one, and it is illustrated in Figure 5.2. It consists of a conventional, direct grid coupled squirrel cage induction generator, which is coupled to the aerodynamic rotor through a speed increasing gearbox [1], [42]. The gearbox is used because the optimal rotor and generator speed ranges are different.

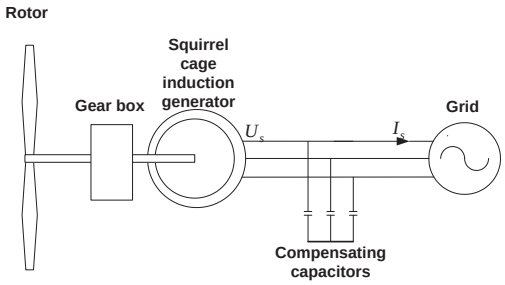

Figure 5.2: Squirrel cage induction generator is used in wind turbines as generating system.

The slip, and also the rotor speed of a squirrel cage induction generator vary with the generated power. These rotor speed variations are, very small. Therefore, the turbine is normally considered to operate at constant speed. Because of the squirrel cage induction generator consumes reactive power, capacitors are often added to generate magnetizing currents in the case of large wind turbines and/or weak grids, and improving the power factor of the system. The power extracted from the wind needs to be limited, because otherwise the generator could be overloaded or the pullout torque could be exceeded, leading to rotor speed instability [43], [42]. In such case, this is often done by using the stall effect. This means that the rotor geometry is designed in such a way that its aerodynamic properties make the rotor efficiency decrease in high wind speeds, thus limiting the power extracted from the wind and preventing the generator from being damaged and the rotor speed from becoming unstable. Thus, during normal operation of a stall regulated wind turbine no controllers are reactive.

5.2.2 Doubly Fed (Wound Rotor) Induction Generator and Direct Drive Synchronous Generator

Figure 5.3 shows the other two generating systems. They are used in variable speed turbines. With these it is possible to increase the energy captured by the aerodynamic rotor by maintaining the optimum power coefficient over a wide range of wind speeds [42]. However it is then necessary to decouple the speed of the rotor from the frequency of the grid through some form of power electronic converters. In the doubly fed induction generator, a back-to-back voltage source converter feeds the three phase rotor winding. In this way, the mechanical and electrical rotor frequencies are decoupled and the electrical stator and rotor frequency can be matched, independently of the mechanical rotor speed. In the direct drive synchronous generator, the generator is completely decoupled from the grid by a power electronics converter. The grid side of this converter is a voltage source converter, i.e. an IGBT (Insulated Gate Bipolar Transistor) bridge. The generator side can either be a voltage source converter or a diode rectifier. The generator is excited using either an excitation winding or permanent magnets.

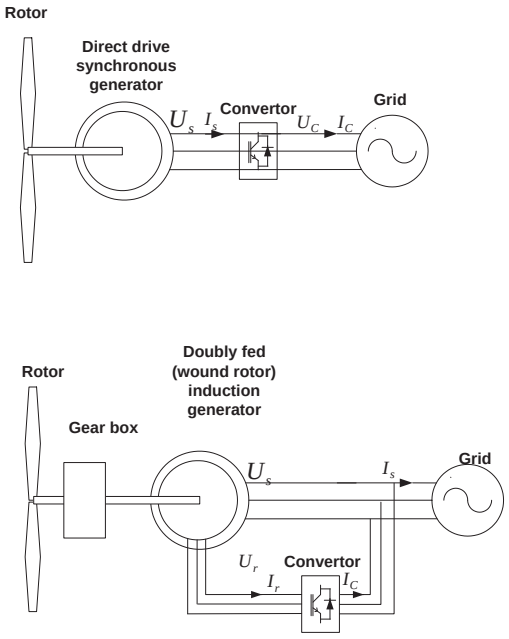

Figure 5.3: Generating systems used in wind turbines: direct synchronous generator and doubly fed (wound rotor) induction generator.

5.3 Wind Turbine Modelling

In this section, an overview of the developments in wind turbine modelling will be presented. The development of wind turbines (several hundreds of kWs to MWs) is addressed. The first wind turbines were based on a direct grid coupled synchronous generator with pitch controlled rotor blades to limit the mechanical power in high wind speeds. Therefore, the first modelling efforts were devoted to this wind turbine concept [44], [42].

The directly grid coupled synchronous generator was followed by the directly grid coupled asynchronous squirrel cage induction generator. This type of generator has a more favorable

torque versus speed characteristic than the synchronous generator, thus reducing the mechanical loads and it is also cheaper. This concept is still applied nowadays by some manufacturers. To limit the power extracted from the wind at high wind speeds, either pitch control or stall control can be applied. Many papers on modelling of a wind turbine with a directly grid coupled squirrel cage induction generator can be found in the literature, both in combination with pitch control and with stall control of the mechanical power, e.g. [45].

The problems with design of the pitch control result that the wind turbine with a directly grid coupled squirrel cage induction generator and pitch control does no longer appear in the product portfolio of any manufacturer. It has appeared to be rather difficult to limit the output power to the nominal value by controlling the pitch of the rotor blades. Thus, although models and analysis of a wind turbine with a directly grid coupled squirrel cage induction generator still appear in journals and conference proceedings now and then, the value of these is rather limited [46].

Nowadays, the more modern variable speed wind turbine with a doubly fed induction generator has replaced of the conventional constant speed wind turbine with a directly grid coupled squirrel cage induction generator. The manufacturers have also started to apply a direct drive synchronous generator grid coupled through a power electronic converter of the full generator rating. Therefore, modelling efforts have been given to these wind turbine concepts as well. Because the variable speed wind turbines are complicated systems, most papers addressing their modelling only cover one subsystem, such as the electromechanical conversion system , the drive train, the control of the generator currents and the DC link voltage or the rotor speed controller, e.g. [47].

As the power developed is proportional to the cube of the wind speed it is obviously important to locate any electricity generating turbines in areas of high mean annual wind speed, and the available wind resource is an important factor in determining where wind farms are sited [1]. Often the areas of high wind speed will be away from habitation and the associated well-developed electrical distribution network, leading to a requirement for careful consideration of the integration of wind turbines to relatively weak electrical distribution networks. The difference in the density of the working fluid(water and air) illustrates clearly why a wind turbine rotor of a given rating is much larger in size than a hydro-turbine [1].

5.3.1 Rotor Equation

A wind turbine operates by extracting kinetic energy from the wind passing through its rotor. The power developed by a wind turbine is given by:

$$P = {}^{1}\!/_{2} C_p \vartheta V_w^3 A \tag{5.1}$$

where:
P = Power (W).
C_p = power coefficient.
V_w = Wind velocity (m/s).
A = swept area of rotor disc(m^2).
ϑ = density of air (1.225 kg/m^3).
The force extracted on the rotor is proportional to the square of the wind speed and so the

wind turbine must be designed to withstand large forces during storms. Most of modern designs are three-bladed horizontal-axis rotors as this gives good value of peak C_p together with an aesthetically pleasing design [1].

The power coefficient C_p is a measure of how much of energy in the wind is extracted by the turbine. It varies with rotor design and the relative speed of the rotor and wind (known as the tip speed ratio) to give a maximum practical value of approximately 0.4 [1]. The power coefficient C_p is a function of the tip speed ratio λ and the pitch angle β, which will be investigated further. The calculation of the performance coefficient requires the use of blade element theory [48],[42]. As this requires knowledge of aerodynamics and the computations are rather complicated, numerical approximations have been developed[44]. Here the following function will be used:

$$C_p(\lambda,\beta) = 0.5176(\frac{116}{\lambda_i} - 0.4\beta - 5)e^{\frac{-21}{\lambda_i}} + 0.0068\lambda \tag{5.2}$$

with

$$\frac{1}{\lambda_i} = \frac{1}{\lambda + 0.08\beta} - \frac{0.035}{\beta^3 + 1} \tag{5.3}$$

Figure 5.4 shows the $C_p(\lambda,\theta)$ versus λ characteristics for various values of β. Using the actual values of the wind and rotor speed, which determine λ, and the pitch angle, the mechanical power extracted from the wind can be calculated from equations (5.1) to (5.3). The maximum value of C_p (c_{pmax}=0.48) is achieved for $\beta = 0°$ and for $\lambda = 8.1$. This particular value of λ is defined as the nominal value (λ_{nom}).

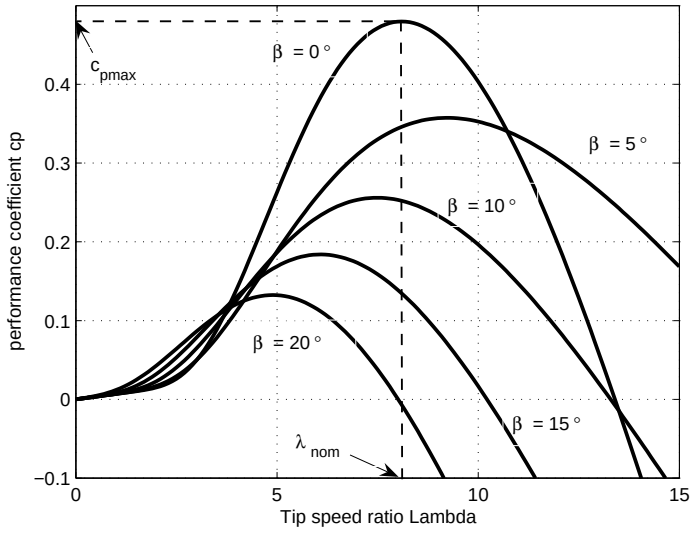

Figure 5.4: Performance coefficient C_p as a function of the tip speed ratio λ with pitch angel β as a parameter .

5.3.2 Generator Equation

Generator is the device converting mechanical energy into electricity, so it is important to the whole system. The equation describing the doubly fed induction machine can be found in [49]. When modelling the doubly fed induction generator, the generator convention will be used,

which means that the currents are outputs instead of inputs and the real power and reactive power have positive signs when they are fed into the grid. By using the generator convention, the following set of equations are obtained [43]:

$$\begin{aligned} v_{ds} &= -R_s i_{ds} - \omega_s \psi_{qs} + \frac{d\psi_{ds}}{dt} \\ v_{qs} &= -R_s i_{qs} + \omega_s \psi_{ds} + \frac{d\psi_{qs}}{dt} \\ v_{dr} &= -R_r i_{dr} - s\omega_s \psi_{qr} + \frac{d\psi_{dr}}{dt} \\ v_{qr} &= -R_r i_{qr} + s\omega_s \psi_{dr} + \frac{d\psi_{qr}}{dt} \end{aligned} \tag{5.4}$$

where

v is the voltage in [V].

i is the current in [A].

R is the resistance in [Ω].

ω_s is the stator electrical frequency in [rad/s].

ψ is the flux linkage in [Vs].

s is the rotor slip.

Subscripts d and q are direct and quadrature axis components respectively; subscripts s and r indicate the stator and the rotor quantities. All the quantities in equation (5.4) are functions of time. The d-q reference frame is rotating at synchronous speed with the q- axis 90° ahead of the d-axis. The position of the d-axis coincides with the maximum of the stator flux, which means that v_{qs} equals the terminal voltage e_t and v_{ds} equals to zero. The flux linkages can be calculated using the following set of equations in per unit [43].

$$\begin{aligned} \psi_{ds} &= -(L_s + L_m) i_{ds} - L_m i_{dr} \\ \psi_{qs} &= -(L_s + L_m) i_{qs} - L_m i_{qr} \\ \psi_{ds} &= -(L_r + L_m) i_{dr} - L_m i_{ds} \\ \psi_{qr} &= -(L_r + L_m) i_{qr} - L_m i_{qs} \end{aligned} \tag{5.5}$$

where L_m is the mutual inductance and L_s and L_r are the stator and rotor leakage inductances, respectively. In equation(5.5) the generator convention is used again. The rotor slip is defined as [43]:

$$s = \frac{\omega_s - \frac{P}{2}\omega_m}{\omega_s} \tag{5.6}$$

where P is the number of poles and ω_m is the mechanical frequency of the generator in [rad/s].

From equations 5.4, 5.5, we can derive the voltage current relationships of the doubly fed induction generator.

Reference [43] proposes that the rotor and stator transients, represented by the last term in equation (5.4) are to be neglected. Substituting (5.5)in to (5.4)results in:

$$\begin{aligned} v_{ds} &= -R_s i_{ds} + \omega_s((L_s + L_m) i_{qs} + L_m i_{dr}) \\ v_{qs} &= -R_s i_{qs} - \omega_s((L_s + L_m) i_{ds} + L_m i_{dr}) \\ v_{dr} &= -R_r i_{dr} + s\omega_s((L_r + L_m) i_{qr} + L_m i_{qs}) \\ v_{qr} &= -R_r i_{qr} + s\omega_s((L_r + L_m) i_{dr} + L_m i_{ds}) \end{aligned} \tag{5.7}$$

The active power P and reactive power Q generated by the generator can be written as:

$$\begin{aligned} P &= v_{ds}i_{ds} + v_{qs}i_{qs} + v_{dr}i_{dr} + v_{qr}i_{qr} \\ Q &= v_{ds}i_{ds} - v_{qs}i_{qs} + v_{dr}i_{dr} - v_{qr}i_{qr} \end{aligned} \tag{5.8}$$

From this equation, it can once more be concluded that the reactive power Q is not necessarily equal to the generated reactive power fed into the grid. Equations (5.7) and (5.8) describe the electrical part the generator. However, also the mechanical part must be taken into account in a dynamic model. The following expression gives the electromechanical torque developed by the generator:

$$T_e = \Psi_{dr}i_{qr} - \Psi_{qr}i_{dr} \tag{5.9}$$

The changes in generator speed that result from a difference in electrical and mechanical torque can be calculated using the generator equation of motion

$$\frac{d\omega_m}{dt} = \frac{1}{2H_m}(T_m - T_e) \tag{5.10}$$

in which H_m is the equivalent inertia constant of the generator rotor [s] and T_m is the mechanical torque [p.u.].

Figure 5.5 shows the speed- power turbine curve which reflects both the aerodynamic power and the generated power. At low wind speeds, the output power is too low to be exploited. Normally turbines are started when the wind speed exceeds 3-4 m/s. We can see also that the wind turbine started at 5 m/s and the output power increases with the cube of the wind speed until the rated wind speed is reached.

At wind speeds from 12 m/s to 25 m/s the power is limited to the rated power of the wind turbines by means of stall-regulation or pitch-control. At wind speed over 20-25 m/s wind turbines are normally stopped to avoid high mechanical loads. The wind speed at which wind turbines are stopped is called cut-out speed.

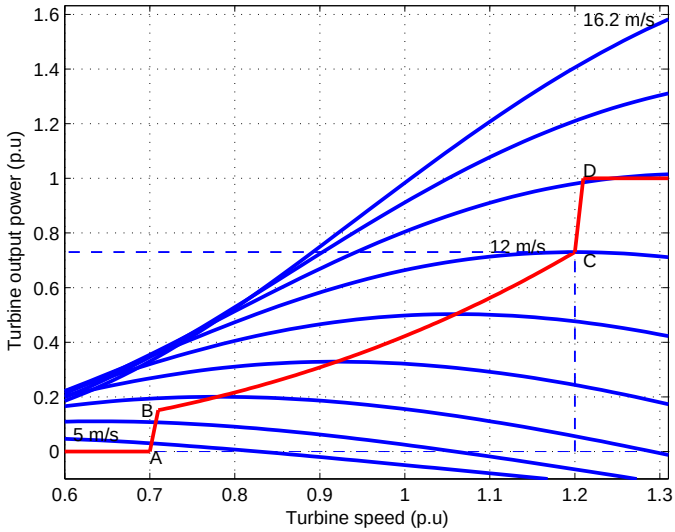

Figure 5.5: Power curve of wind turbine.

5.3.3 Simulation Results

In this section we will examine the behavior of the wind turbine when the wind speed changes. The speed will be first constant 8(m/s), then at time 5 seconds a ramp is introduced lasting until 10 seconds and then constant speed of 14(m/s) follows, as illustrated in Figure 5.6.

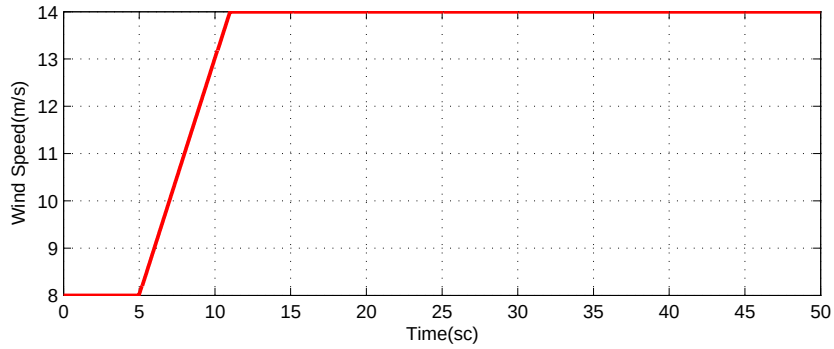

Figure 5.6: Wind Speed.

Figure 5.7 shows the active power P. The generated active power starts increasing smoothly (together with the turbine speed) to reach its rated value of 1.5 MW in approximately 19 s.

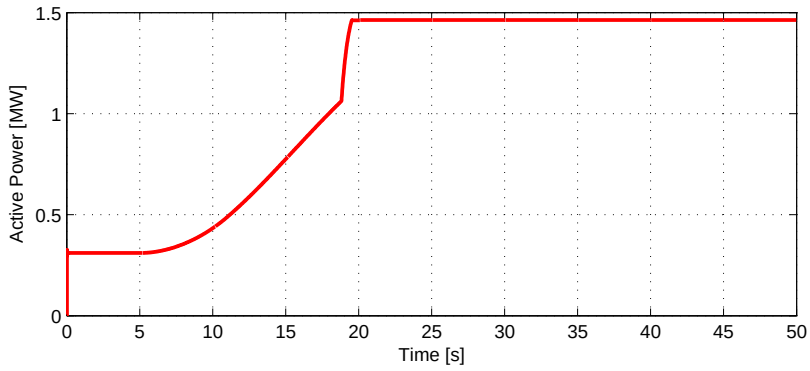

Figure 5.7: Generated active power P.

The response of the reactive power due to a change in the wind speed is shown in Figure 5.8. It can be seen that at nominal power, the wind turbine absorbs 0.11 Mvar (generated Q = -0.11 Mvar).

Figure 5.9 shows the pitch angle response due to the change in the wind speed. In this figure, it is clear that, initially, the pitch angle of the turbine blades is zero degrees and the turbine operating point follows the red curve of the turbine power characteristic up to point D. Then the pitch angle is increased from 0 deg to 0.078 deg in order to limit the mechanical power.

In Figure 5.10 the turbine speed increased when the wind speed increased from 0.8 pu to 1.21 pu.

To simulate the wind turbine responses for different values of wind speed, the initial wind speed is below the nominal wind speed which is assumed to be 14 m/s. After 7 s a wind speed ramp starts which leads to an increase in the average wind speed in 30 s after a 10 s a wind gust with an amplitude of -3 m/s and duration of 10 s occurs [50].

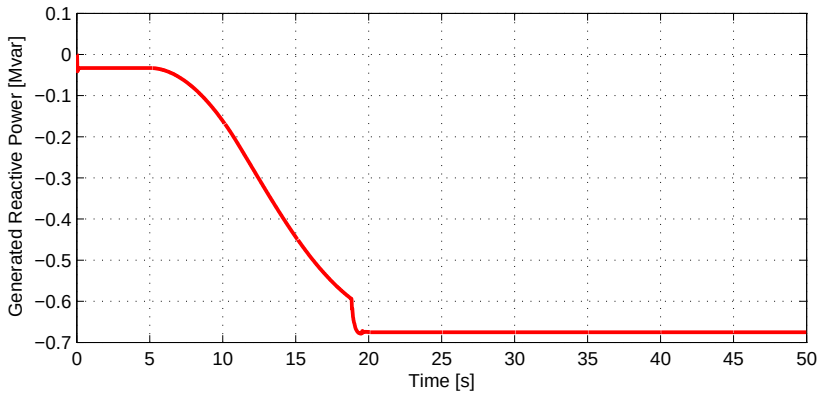

Figure 5.8: Generated reactive power Q.

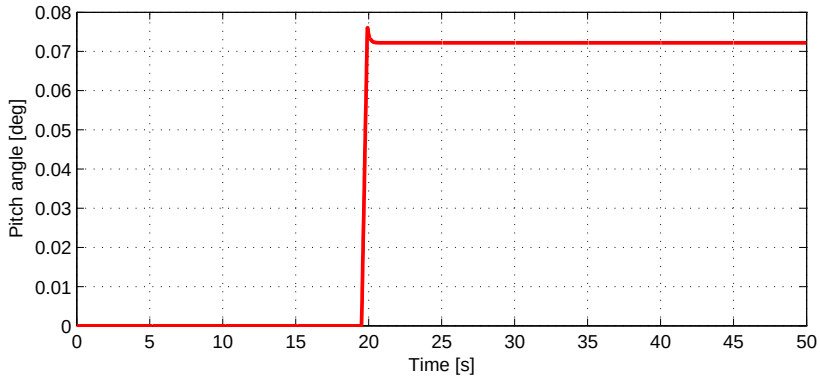

Figure 5.9: Pitch Angle.

The results are illustrated in Figure 5.11 - 5.13. At 20 s, the nominal power of the wind turbine is reached because the pitch angle controller is not used which can prevent the rotor overspeeding.

Next the responses of measured wind sequences is to be simulated. Figures 5.15- 5.17 show the responses of the active power, the pitch angle, and the rotor speed due to the the input measured wind speed 5.14 . The wind speed measurements were downloaded from "Database of Wind Characteristics" which is located at DTU Denmark [51].

It can be seen from the results that the response from the simulated input and measured input wind speed have almost the same range fluctuations of the output power , the range of the response of the rotor speed fluctuations are similar, and the behavior of the response of the pitch angle are different as there were no pitch controller in the design model.

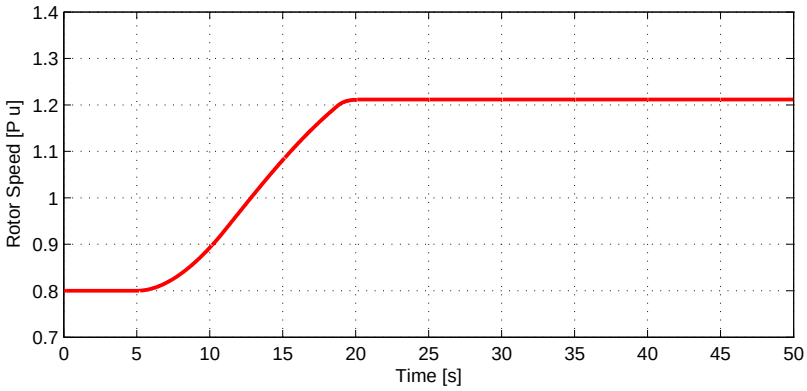

Figure 5.10: Rotor Speed.

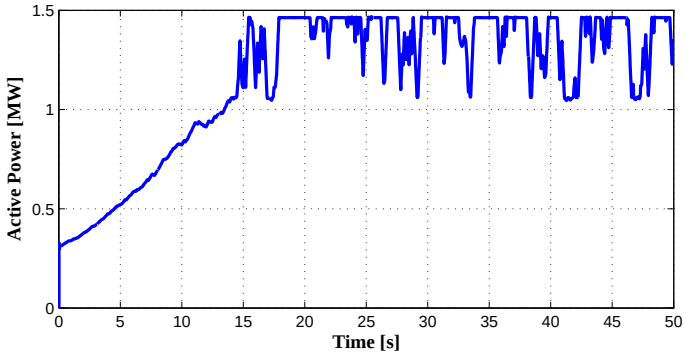

Figure 5.11: Generated active power due to different values of wind speed.

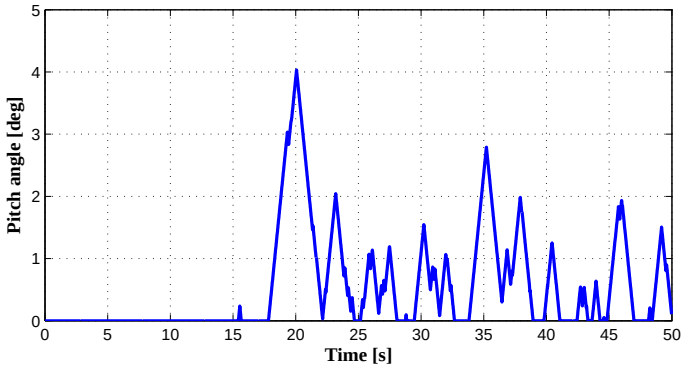

Figure 5.12: Pitch Angle due to different values of wind speed.

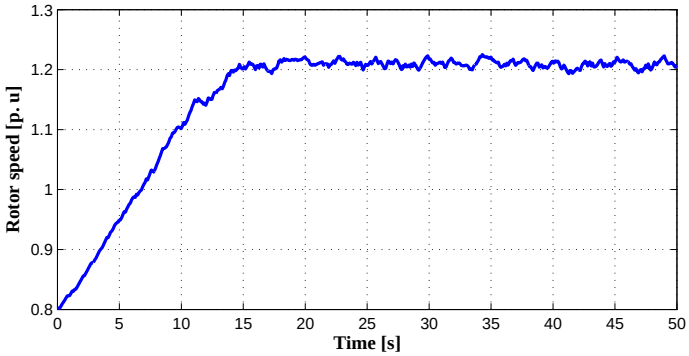

Figure 5.13: Rotor Speed due to different values of wind speed.

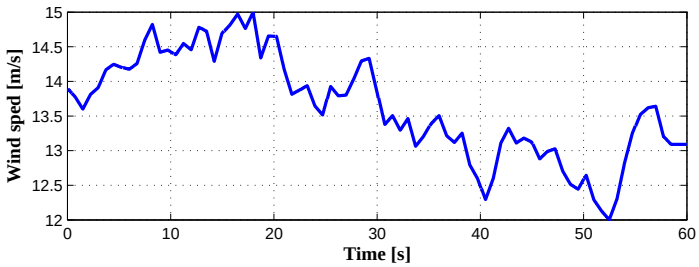

Figure 5.14: Measured sequence wind speed.

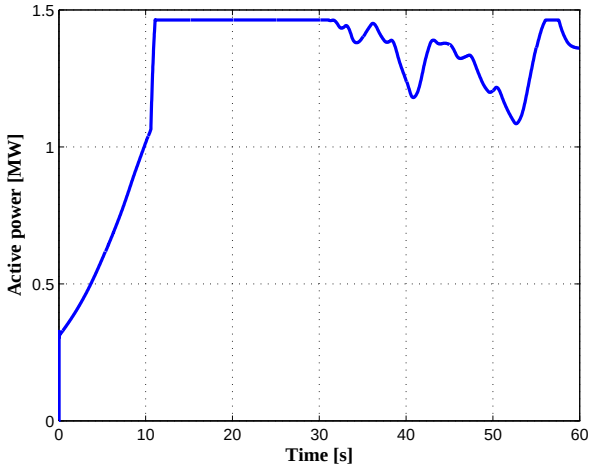

Figure 5.15: Response of the generated active power due to the measured sequence wind speed input .

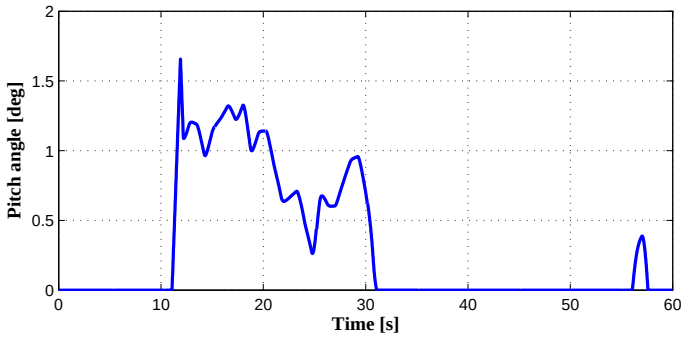

Figure 5.16: Response of the pitch angle due to measured sequence wind speed input.

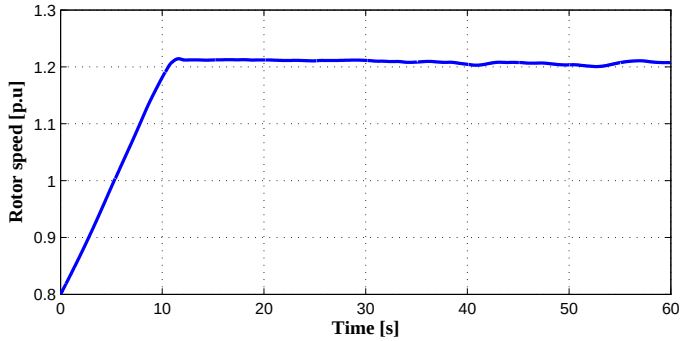

Figure 5.17: Response of the rotor speed due to measured sequence wind speed input.

Chapter 6

Photovoltaic Cell

6.1 Introduction

The photovoltaic (PV) generation systems are expected to increase significantly worldwide. PVs are an attractive source of renewable energy for distributed urban power generation due to their relatively small size and noiseless operation. PV generating technologies have the advantage that more units can be added to meet load increase demand.

Major advantages of the photovoltaic power are as follows [52]:

- Short lead time to design, install, and start up a new plant.
- Highly modular, hence, the plant economy is not a strong function of size.
- Power output matches very well with peak load demands.
- Static structure, no moving parts, hence, no noise.
- High power capability per unit of weight.
- Longer life with little maintenance because of no moving parts.
- Highly mobile and portable because of light weight.

Photovoltaic generation are systems which convert the sunlight directly to electricity. PV technology is well established and widely used for power supplies to sites remote from the distribution network [1].

Photovoltaic cells can be divided into four groups: crystalline cells, thin-film cells, dye-sensitised solar cells (DYSC or Grätzel-cell) and multilayer cells. The latter can also be considered as several layers of thin-film PV cells. The different types are described in [53].

Figure 6.1 shows the schematic diagram of an inverter for small PV grid connected system. The inverter typically consists of the following:

- Maximum power point tracking (MPPT) circuit.
- Energy storage element, usually a capacitor.
- DC:DC converter to increase the voltage.
- DC:AC inverter stage.

- Isolation transformer to ensure that DC is not injected into the network.
- Output filter to restrict the harmonic currents passed into the network.

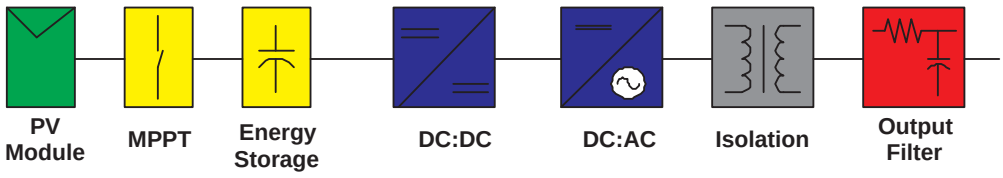

Figure 6.1: Schematic diagram of small PV inverter for grid connected operation.

6.2 Modelling

An initial understanding of the performance of a solar cell may be obtained by considering it as a diode in which the light energy, in form of photons with the appropriate energy level, falls on the cell and generates electron-hole pairs. The electrons and holes are separated by the electric field established at the junction of the diode and are then driven around an external circuit by this junction potential. There are losses associated with the series and shunt resistance of the cell as well as leakage of some of the current back across the p-n junction. This leads to the equivalent circuit of Figure 6.2 [1], [54].

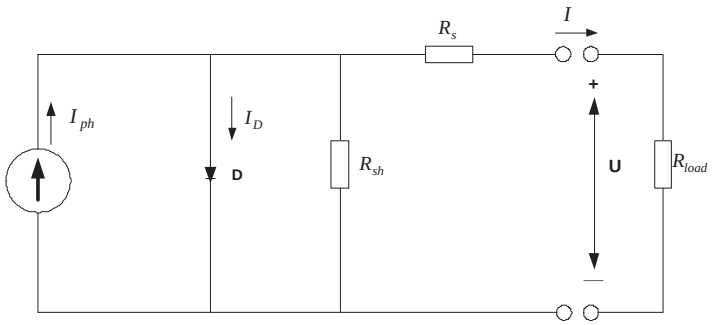

Figure 6.2: Equivalent circuit of a PV module.

The PV cell can be modeled as a diode in parallel with a constant current source and a shunt resistor. These three components are in series with the series resistor.

The output-terminal current I is equal to the light-generated current I_{ph} , less than the diode-current I_D and the shunt-leakage current I_{sh}.

$$I = I_{ph} - I_D - I_{sh} \tag{6.1}$$

The series resistance R_s represents the internal resistance to the current flow, and depends on the p-n junction depth, the impurities and the contact resistance. The shunt resistance R_{sh} is inversely related to the leakage current to the ground. In an ideal PV cell, R_s = 0 (no series loss), and $R_{sh} = \infty$ (no leakage to ground). The PV cell conversion efficiency is sensitive to small variations in R_s , but is insensitive to variations in R_{sh} . A small increase in R_s can decrease the PV output significantly. In the equivalent circuit, the current delivered to the external load equals the current I_{ph} generated by the illumination, less than the diode current I_D and the

ground-shunt current I_{sh} . The open circuit voltage U_{oc} of the cell is obtained when the load current is zero, i.e., when I = 0, and is given by the following:

$$U_{oc} = U + IR_s \tag{6.2}$$

where U is the terminal voltage of the cell [V].
The diode current is given by the classical diode current expression [52]:

$$I_D = I_d \left[\frac{qU_{oc}}{A_{cf} K_B T} - 1 \right] \tag{6.3}$$

where I_D = the saturation current of the diode

q = the electron charge $= 1.6 * 10^{-19}$ Coulombs

A_{cf} = curve fitting constant

K_B = Boltzmann constant $= 1.38 * 10^{-23}$ Joule/°KT

T = temperature [°K].
The load current is given by the expression:

$$I = I_{ph} - I_{os} \left\{ \exp \left[\frac{qU_{oc}}{AKT} \right] - 1 \right\} - \frac{U_{oc}}{R_{sh}} \tag{6.4}$$

where

$$I_{ph} = \frac{G}{100} \left[I_{SCR} + K_I (T - 25) \right] \tag{6.5}$$

$$I_{os} = I_{or} \left(\frac{T}{T_r} \right)^3 \exp \left[\frac{qE_{GO}}{BK} \left(\frac{1}{T_r} - \frac{1}{T} \right) \right] \tag{6.6}$$

and
I,V= cell output current and voltage.
I_{os}= cell reverse saturation current.
q = electron charge=1.6*10^{-19} Coulombs.
A,B= ideality factor of p-n junction.
K=Bolzmann constant.
T=cell temperature [$°C$].
K_I= short circuit current temperature coefficient at I_{SCR},K_I= 0.0017 $A/°C$.
G= solar irradiation in W/m^2.
I_{SCR}= short circuit current at 25$°C$ and 1000W/m^2.
I_{ph}= light generated current.
E_{GO}=band gap for silicon.
T_r=reference temperature, T_r=301.18$°K$.
I_{or}=cell saturation current at T_r.
R_{sh}=shunt resistance.

R_s=series resistance.

I_{SCR}, the current at maximum power point (I_{mpp}), the voltage at maximum power point (V_{mpp}), and the open circuit voltage of the cell U_{oc}, are given by the manufacturers. Table 6.1 illustrates the Standard Test Condition (STC) of AM1.5, $1000W/m^2$ and $25°C$, also the date for 80W PHOTOWATT which is used for the simulation study [55]

Table 6.1: Parameters for 80W photowatt panel PWZ750 at STC.

Parameter	Value
Maximum Power Point, (P_{mpp})	80W
Minimum Power Point, (P_{min})	75.1W
Current at MPP,(I_{mpp})	4.6A
Voltage at MPP,(V_{mpp})	17.3V
Short Circuit Current,(I_{SCR})	5A
Open Circuit Voltage,(U_{oc})	21.9V
Short circuit current temperature coefficient,α_{scT}	$1.57mA/°C$
Open circuit voltage temperature coefficient,β_{ocT}	-78.2$mV/°C$
NOCT (Normal Operating Cell Temperature)	$45°C$
Insolation, G=0.8W/m^2, T_a=20$°C$,wind speed=1m/s	

6.3 Simulation Results

The I-U and P-U characteristics for various irradiance at fixed temperature (T=25 $°C$), obtained from the model are shown in Figures 6.3 and 6.4, respectively.

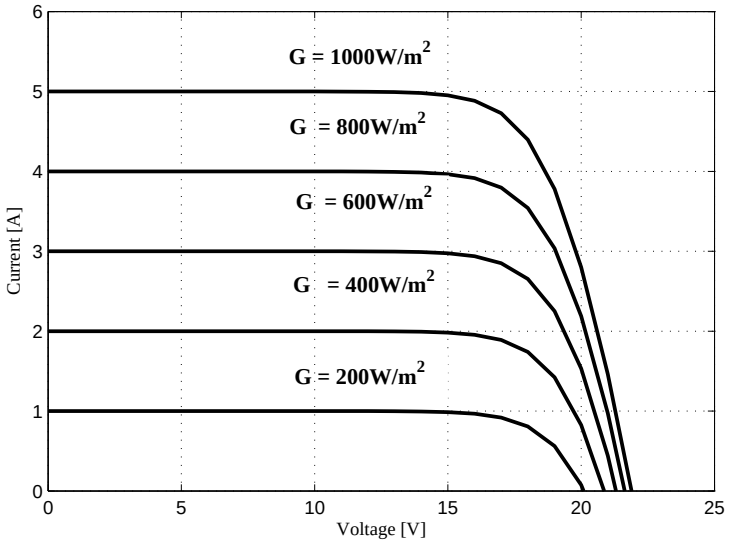

Figure 6.3: I-U characteristic for a PV cell at a constant temperature of $25°C$

Figures 6.5, 6.6 show the I-U characteristics for different values of temperature and fixed irradiance of $1000W/m^2$ respectively.

From the figures, we can conclude that when the irradiation is $1000W/m^2$, which corresponds approximately to a cloud-free, sunny day, the upper curve shows that the open-circuit voltage of the cell is about 22 Volt. As the load (current) of the cell increases, the voltage de-

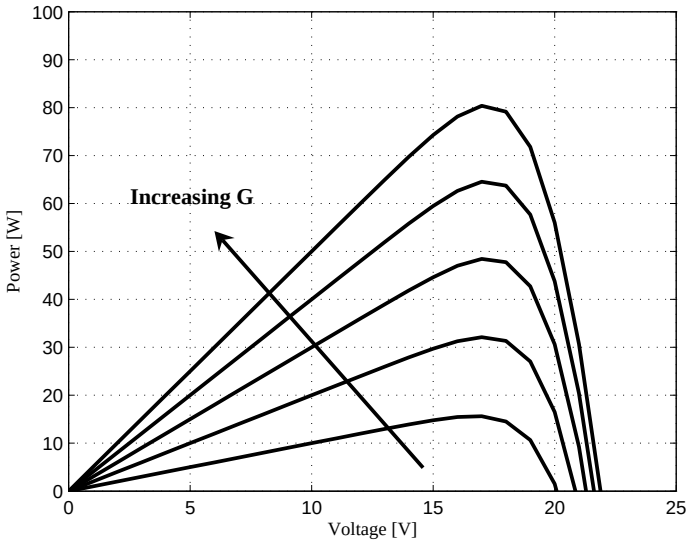

Figure 6.4: P-U characteristic for a PV cell at a constant temperature of $25°C$

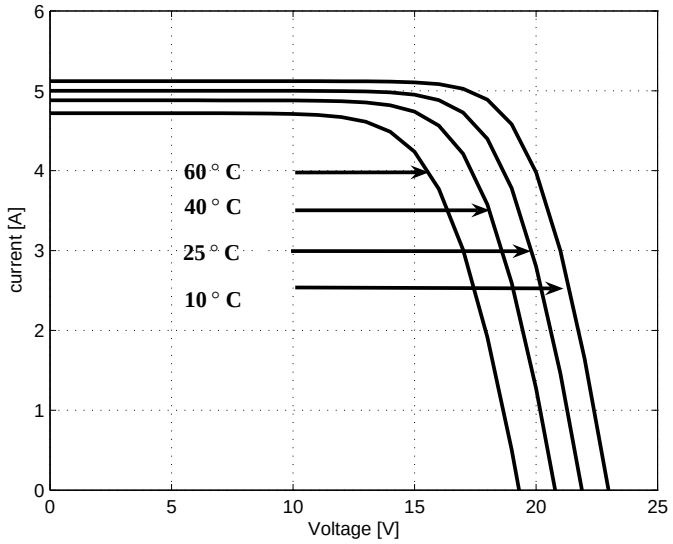

Figure 6.5: I-U characteristic for a PV cell at constant G= $1000W/m^2$

creases and at short-circuit (voltage = 0) the current is approximately 5 A. At open circuit and at short-circuit, no power is produced. At a point called the maximum power point (MPP), maximum power is gained from the PV-cell. To visualise this, a rectangle can be drawn from a point on the curve to the x and y-axis. For the point where this rectangle has the largest area, the maximum power is generated. At a lower irradiation, the short-circuit current decreases approximately linearly with irradiation. The open circuit voltage does not decrease as much until a very low irradiation. However, the open circuit voltage is much more affected by the temperature of the PV-cell. At a higher temperature, the open circuit voltage decreases. The phenomenon has quite a large impact and it decreases the output power by approximately 15 $\%$ at a temperature increase from $25°C$ to $60°C$.

The effect of irradiance and cell temperature on I-V characteristic curve is shown in Figures

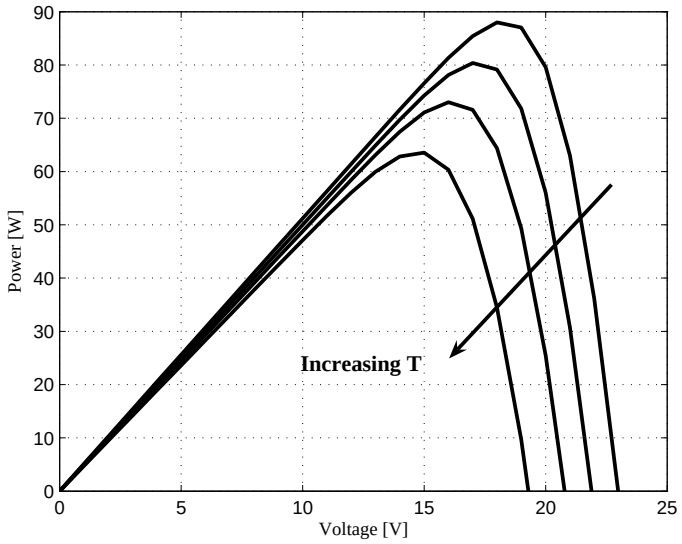

Figure 6.6: P-U characteristic for a PV cell at constant G= $1000W/m^2$

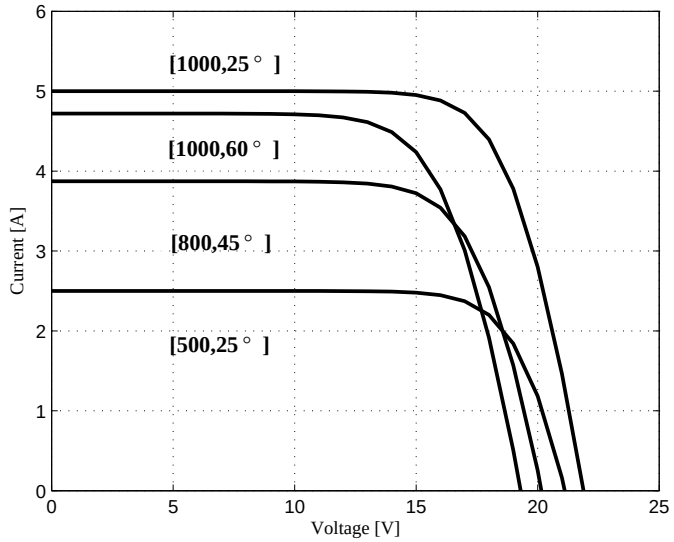

Figure 6.7: I-U characteristic of PV for some set of G and T

6.3 and 6.5. Figure 6.3 shows that the maximum power output varies almost linearly with the irradiance. Figure 6.5 shows that the maximum output power from the PV decreases as the temperature increases.

Chapter 7

Conclusions and Future Work

7.1 Conclusions

In this final chapter, the importance, aims and outcomes of this research are highlighted and summarized. The research is discussed in terms of what it aims for and how it could contribute to the power industry's needs. It also explores, how the research could be extended and improved and how this might be done. This includes what can be done in the future to understand MG behavior.

It is hoped that by making optimal use of the small and varied energy sources which comprise MGs, MGs may be able to make a significant contribution to the distributed power generation. For instance, if the sun is out, the PV array may provide power; if it is windy the wind turbine will generate the power; if it is neither or if more power is needed, the fuel cell, diesel engine, and micro-turbine or main supply can be used. The inclusion of batteries in a MG system allows excess power produced to be stored, or alternatively, the excess power could be put into the main grid. In this way it is expected that MGs could reduce pollution and deliver reliable energy in a variety of situations as discussed in Chapter 1.

Microgrid behaviour on the whole is not well understood. For this reason the thesis aims to develop models suitable for overall analysis and design. The aim of the work was to model both the transient and the steady-state behaviour of the MG's individual power sources. The final goal was to lay a groundwork which would allow analysis for the further development of a more complete model. More specifically, models of a diesel engine, fuel cell, photovoltaic cell, a micro-turbine and a wind turbine have been developed. This work has been successful in accomplishing theobjective. All models developed will allow for investigation that will provide an understanding of MGs to facilitate the evolution of a more sophisticated model.

7.1.1 Modelling of the Diesel Engine

From control system point of view, a diesel engine can be considered as a speed-feedback system. After the operator gives a speed command through adjusting the governor setting, the engine governor which is also working as a sensor, will recognize the difference between the actual speed and the desired speed, and regulates the fuel supply to maintain the engine speed within range.

The general structure of the fuel actuator system is usually represented as a first order phase-

lag network., which is characterized by gain, and time constant. Figure 2.1, and equation 2.1 show the actuator and the current driver constant. The output of the actuator is the fuel-flow. Fuel flow is then converted to a mechanical torque after a time delay and engine torque constant, which can be represented by the model of the diesel engine as shown in Figure 2.2, and equation 2.2.

Based on the results of this work it can be concluded that control of the speed of the diesel engine using the genetic algorithm based on RLS and PID controller can control the system efficiently. The proposed controller procedure seems to control the system even if the system has a time delay variation and load injection. The optimal controller obtained using the genetic algorithm is far more efficient than that used in [15], [17], and [19] as overshoot, rise time and settling time are greatly reduced. Load injection does not affect the resulting controller. The response for the system shows good performance in reducing the overshoot, rise time, and settling when the load applied. Moreover, it was shown that the proposed method was effective in controlling the speed of the diesel engine. Genetic algorithm was proven to be an efficient way of finding optimal controller.

Another useful characteristic of genetic algorithms relevant to our controllers is that they can be used to obtain a controller with specific specification. Objective functions can be used to specify certain overshoots, rise time and settling times. For example, multi-objective optimization could also be used. There could be an evaluation function for calculating fitness and another evaluation function to make sure that the PID values conform to a specific standard. An example of this would be to reject PID values that cause an overshoot greater than what is desired.

7.1.2 Modelling of Fuel Cell

Dynamic responses of the output power, voltage, current are obtained by modelling Solid Oxide Fuel Cell (SOFC). The responses of pressure difference between hydrogen and oxygen could also be studied. The response time of a SOFC is limited by the time constants of the fuel processor, which are normally large and cannot be made smaller for a given fuel cell due to physical limitations imposed by the parameters of the corresponding chemical reactions. Therefore, the response time of the plant cannot be enhanced by manipulating its input. Technological changes in the fuel cell plant are required if the fuel cell power plant is to operate in a stand alone mode, which requires load-following capabilities. Alternatively, other technical solutions should be sought; for example, the combined use of fuel cell modules and a gas turbine, or the use of an external energy storage, such as batteries, a flywheel, or a superconducting magnetic energy storage device.

The developed SOFC system model appears suitable for the time scale to be used in our dynamic simulation.

7.1.3 Modelling of MicroTurbine

The microturbine model has been developed to investigate the responses of the output power, shaft speed, DC link voltage for different levels of power demand. The simulated model and the results obtained for various operating conditions permit to predict the performance of the microturbine. The simulation results demonstrate that the established model provides a useful

tool suitable to study and to perform accurate analysis of most electrical phenomenon that occurs when a microturbine is connected to the grid. The simulation results obtained for different levels of power demand show the usefulness of the model and its accuracy. The aim of future work will be to investigate more questions such as islanding operation.

7.1.4 Modelling of Wind Turbine with Doubly Fed Induction Generator

Modelling of the wind turbine with a doubly fed induction generator and also the development of models of the most important current wind turbine types for power system dynamics simulations was completed. First, the basic working principle of the wind turbine was discussed. Then, an overview over the most important types of wind turbines was given: they are constant speed wind turbine with a squirrel cage induction generator, and the variable speed wind turbine with a doubly fed induction generator and the one with a direct drive synchronous generator. The structure of the model of each of these turbine types was depicted, after which equations for each of the subsystems were given. Finally, the models were used in simulations in order to investigate the impact of changing the wind speed on the active power, pitch angel, rotor speed, also to study the power curve of the wind turbine. Measured wind sequence data is used to see the responses of active power, rotor speed, pitch angle. Wind turbine responses a with designed signal which it has different values of wind speed were also simulated. From these it can be seen that the responses from the simulated input and measured input wind speed have almost the same range fluctuations of the output power, the range of the response of the rotor speed fluctuations are similar, the behavior of the response of the pitch angle is different as there were no pitch controller in the design model.

7.1.5 Modelling of Photovoltaic Cell

Having a simple but equivalent model of a photovoltaic cell allows the extraction of the device's electrical characteristics. The model is presented and analyzed. The current voltage relationship of the PV is determined by the shunt and series resistances and the magnitude of the current source. From the equations modeling the PV, it can be seen that the open circuit voltage is logarithmically proportional to the magnitude of the current source. The short circuit current is directly proportional to illumination intensity. The solar cell current ranges from zero to short circuit current. The solar cell voltage ranges from zero to open circuit voltage, U_{oc} . As current increases, the voltage decreases due to the series resistance. As the voltage increases, the current decreases due to the shunt resistance. Since power is the product of voltage and current, the current that will produce the maximum power current will be found to be somewhere between zero and the short circuit current, and the maximum power voltage will be found somewhere between 0 and U_{oc} .

The results are thus satisfactory, and it is expected that they will improve through further testing and development. These different sources will be connected together to form a microgrid. It is anticipated at least two of the three power sources will be connected together to power a single load

7.2 Microgrid Modelling and the Future

The next step in research is to consider MG as a system. It is important to learn more about how the sources interact with each other. More specifically their relationship to each other needs to be defined. If all goes as anticipated and the MG system is developed, the control of the system will likely be imbedded within the electronics. It is possible to use specialised controllers to get a more stable response and to use each power source more efficiently. This should certainly be researched and considered once the power sources interaction and relationship with each other and the mains have been defined. Other aspects that could be developed further are the individual sources within the MG. This could be done at two levels. The first is the consideration of other variables for each source. For example, the wind speed is not considered for the PV array and in some conditions it would prove quite significant. Also, working in pu is more desirable than actual values: the full conversion of the microsources to pu would be useful. The other way is to keep the model up-to-date with the technology. In the area of PV arrays and micro turbines technology is rapidly changing and improving.

The final important aspect is to obtain some actual MG data (rather than data from individual power sources). During this work we were unable to find any actual data from implemented MGs. This is likely due to MGs being such a new idea and therefore no data is currently available.

7.3 Final Remarks and Future Work

In this work, modelling of components of a MG system has been successfully done. Models, which allow for investigation of the individual power sources behaviour have been developed. The work was carried out by doing extensive research and by using a design process to implement each system individually. Testing and development through understanding was also a significant part of this work. The goals of this work have been met and it is anticipated that further research and development will be carried out on the system, with the goal that MGs will be able to make a valid, greener, contribution to the world's growing energy needs.

Bibliography

[1] N. Jenkins, R. Allan, P. Crossley, D. Kirschen, and G. Strbac. *Embedded Generation*. The Institution of Electrical Engineers, UK, 2000.

[2] T.E Hoff, H.J Wenger, and B.K. Farmer. Distributed generation: An alternative to electric utility investments in system capacity. *Energy Policy*, 24(2):137 – 147, 1996.

[3] B. Lasseter. Microgrids [distributed power generation]. In *IEEE Power Engineering Society Winter Meeting, 2001.*, volume 1, pages 146–149, Columbus, Ohio, Feb 2001.

[4] R. Lasseter. Microgrids. In *IEEE Power Engineering Society Winter Meeting, 2002.*, volume 1, pages 305–308, New York, NY, 2002.

[5] Y. Zoka, H. Sasaki, N. Yorino, K. Kawahara, and C.C Liu. An interaction problem of distributed generators installed in a microgrid. In *Proceedings of IEEE on Electric Utility Deregulation, Restructuring and Power Technologies Conference*, volume 2, pages 795 – 799, Hong Kong, April 2004.

[6] Sakis Meliopoulos. Challenges in simulation and design of ţgrids. In *Proceedings of the 2002 IEEE/PES Winter Meeting, New York, NY*, 2002.

[7] G. Venkataramanan and M. Illindala. Microgrids and sensitive loads. In *Proc. IEEE Power Eng. Soc. Winter Meeting, 2002*, volume 1, pages 316–322, 2002.

[8] J.M. Correa, S. Chakraborty, M.G. Simoes, and F.A. Farret. A single phase high frequency ac microgrid with an unified power quality conditioner. In *Proc. IEEE-Industry Applications Conference*, volume 2, pages 956–962, October 2003. Conference Record of the 38th IAS Annual Meeting, SaltLake City, UT.

[9] P. P. Barker and B. K Johnson. Power system modeling requirements for rotating machine interfaced distributed resources. In *Power Engineering Society Summer Meeting*, volume 1, pages 161–166, July 2002.

[10] S. Blazwicz and D. Kleinschmidt. Distributed generation: System interface. [Online]. Available: http://www.encorp.com/dwnld/pdf/whitepaper/wp_ADL_2.pdf, May 1999.

[11] T. Ackermann and V. Knyazkin. Interaction between distributed generation and the distribution network: operation aspects. In *Transmission and Distribution Conference and Exhibition 2002: Asia Pacific. IEEE/PES*, volume 2, pages 1357–1362, Oct 2002.

[12] A. Amstutz and K. Luigi. EGO sensor based robust output control of EGR in diesel engines. *IEEE Transactions on Control System Technology*, 3(5):39 – 48, March 1995.

[13] S. Häggmark, V. Neimane, U. Axlsson, P. Holmberg, G. Karlsson, K. Kauhaniemi, M. Olsson, and C. Liljergren. Asppects of different distributed generation technologies, CODGUENT WP. March 2003. [Online]. Available: http://www.energia.fi/attachment.asp?Section=1353&Item=10792.

[14] G. S. Stavrakakis and G. N. Kariniotakis. A general simulation algorithm for the accurate assessment of isolated diesel-wind turbines systems interaction. i. a general multimachine power system model. *IEEE Transactions on Energy Conversion*, 10(3):577 – 583, Sept 1995.

[15] B. Kuang, Y. Wang, and Y. L. Tan. An H_∞ controller design for diesel engine systems. In *Power System Technology, International Conference Proceedings*, volume 1, pages 61–66, Dec 2000.

[16] S. Roy, O.P. Malik, and G.S. Hope. A least squares based model fitting identification technique for diesel prime movers with unknown dead time. *IEEE Transactions on Energy Conversion*, 6(2):251 – 256, June 1991.

[17] S. Roy, O.P. Malik, and G.S. Hope. An adaptive control scheme for speed control of diesel driven power-plants. *IEEE Transactions on Energy Conversion*, 6(4):605 – 611, Dec. 1991.

[18] Y. Hu, M. Cirstea, M. McCormick, and L. Haydock. Modelling and simulation of a variable speed stand-alone generator system. In *Proceedings of Power Electronics and Variable Speed Drives, 2000. Eighth International Conference*, pages 372 – 377, Sept. 2000.

[19] S. Roy, O.P. Malik, and G.S. Hope. A k- step predictive scheme for speed control of diesel driven power plant. *IEEE Transactions on Industry Application*, 29(2):389 – 396, March/April 1993.

[20] A. Ozeki, H. Fujikawa, S. Yamada, and H. Tanaka. A design method of self-tuning controller for unknown time-delay system. In *Proceedings Industrial Electronics, Control, Instrumentation, and Automation, 'Power Electronics and Motion Control Conference*, volume 3, pages 1218 – 1223, Tokyo,Japan, Nov 1992.

[21] P. E. Wellstead and M. B. Zarrop. *Self-tuning systems: control and signal processing*. John Wiley & Sons Inc, April 1991.

[22] H. N. Koivo and A. Reijonen. Tuning of PID controller for varying time- delay system. In *Proceedings of the IEEE International Conference on Mechatronics ICM '04*, pages 446 – 451, Istanbul,Turkey, 2004.

[23] K Zenger. *Analysis and Controller Design of Time-Variable Flow Processes*. PhD thesis, Laboratory of Control Engineering, HELSINKI UNIVERSITY OF TECHNOLOGY, 2003. [Online]. Available: http://lib.hut.fi/Diss/2003/isbn9512264390/.

[24] M. Dotoli, G. Maione, D. Naso, and E. B. Turchiano. Genetic identification of dynamical systems with static nonlinearities. In *Proceedings of Mountain Workshop Soft Computing Industrial Applications*, pages 65 – 70, June 2001.

[25] K. Kristinnson and G. A. Dumont. System identification and control using genetic algorithms. *IEEE Transactions on System, Man, Cybern*, 22:1033 – 1046, Sept.-Oct 1992.

[26] C. H. Marrison and R. F. Stengel. Robust control system design using random search and genetic algorithms. *IEEE Transactions on Automatic Control*, 42:835–839, June1997.

[27] F. Cupertino, E. Mininno, D. Naso, B. Turchiano, and L. Salvatore. On- line genetic design of anti- windup unstructured controller for electrical drives with variable load. *IEEE Transactions on Evolutionary Computation*, 8(4):347–363, August 2004.

[28] A.J. Chipperfield, P.J. Flemming, A. Polheim, and C. M Fonscea. *Genetic Algorithm Toolbox*. University of Sheffield. Available: http://www.ie.ncsu.edu/mirage/GAToolBox/gaot/.

[29] W. Morgantown. Fuel Cell Handbook. 6th Edition, EG&G Technical Services, Virginia, November 2002. [Online]. Available: http://www.rwth-aachen.de/lbz/linksframe.html.

[30] J.A. Smith, M.H. Nehrir, V. Gerez, and S.R Shaw. A broad look at the workings, types, and applications of fuel cells. In *Power Engineering Society Summer Meeting*, volume 1, pages 70–75, Chicago, USA, July 2002.

[31] A.R Sakhare, A. Davari, and A. Feliachi. Control of stand alone solid oxide fuel cell using fuzzy logic. In *Proceedings of the 35th Southeastern Symposium on System Theory, 2003.*, pages 473 – 476, 16-18 March. 2003.

[32] M.W. Ellis, M.R. Von Spakovsky, and D.J Nelson. Fuel cell systems: efficient, flexible energy conversion for the 21st century. In *Proceedings of the IEEE*, volume 89, pages 1808 – 1818, Dec. 2001.

[33] J. Padulles, G.W. Ault, C.A. Smith, and J.R. McDonald. Fuel cell plant dynamic modelling for power systems simulation. In *Proceedings of 3dth universities power engineering conference*, volume 34, pages 21–25, 1999.

[34] K. Sedghisigarchi and A. Feliachi. Dynamic and transient analysis of power distribution systems with fuel cells-part i: fuel-cell dynamic model. *IEEE Transactions on Energy Conversion*, 19(2):423 – 428, 2004.

[35] Y. Zhu and K. Tomsovic. Development of models for analyzing the load- following performance of microturbine and fuel cells. *Electric Power System Research journal*, Dec. 2001.

[36] C. Sharma. Modeling of an island grid. *IEEE Transaction on Power System*, 13(3):971–978, August 1998.

[37] W. G. Scott. Micro- turbine generators for distribution systems. *IEEE Industry Applications Magazine*, 4(4):57–62, May/June 1998.

[38] H. Nikkhajoei and M.R. Iravani. Modeling and analysis of a micro-turbine generation system. In *IEEE Power Engineering Society Summer Meeting*, volume 1, pages 167 – 169, Chicago, USA, July 2002.

[39] G. Venkataramanan, M. S. Illindala, C. Houle, and R. H. Lasseter. Hardware development of a laboratory-scale microgrid phase 1–single inverter in island mode operation. In *Base Year Report, December2000 – November 2001*, 2000. NREL Report No. SR-560-32527.

[40] R. Lasseter and P. Piagi. Providing premium power through distributed resources. In *Proceedings of the 33rd Hawaii International Conference on System Sciences.*, volume 1, pages 1–9, Hawaii, Jan 4-7 2000.

[41] R. Lasseter. Dynamic models for micro-turbines and fuel cells. In *IEEE Power Engineering Society Summer Meeting.*, volume 2, pages 761 – 766, British Columbia, Canada, July 2001. NREL Report No. SR-560-32527.

[42] T. Ackermann. *Wind Power in Power Systems*. John Wiley & Sons, Ltd, Royal Institute of Technology, Stockholm Sweden, 2005.

[43] J.G. Slootweg, S.W.H. de Haan, H. Polinder, and W.L. Kling. Modeling wind turbines in power system dynamics simulations. In *Power Engineering Society Summer Meeting, 2001. IEEE*, volume 1, pages 22 – 26, Vancouver,Canada, 15-19July 2001.

[44] J.G. Slootweg. *Wind Power: Modelling and Impact on Power System Dynamics.* PhD thesis, Technische Universiteit Delft, Delft, Netherlands, December 2003.

[45] S.A. Papathanassiou and M.P. Papadopoulos. Mechanical stresses in fixed-speed wind turbines due to network disturbances. *IEEE Transactions on Energy Conversion*, 16(4):362–367, Dec. 2001.

[46] J. Tamura, M. Ueno, Y. Matsumura, and S. Kimoto. Transient stability simulation of power system including wind generator by pscad/emtdc. In *Proceedings of 2001 IEEE Porto Power Tech Conference*, volume 4, Sept. 2001.

[47] F.D. Kanellos, S.A. Papathanassiou, and N.D. Hatziargyriou. Dynamic analysis of a variable speed wind turbine equipped with a voltage source ac/dc/ac converter interface and a reactive current control loop. In *Proceedings of Electrotechnical Conference*, volume 3, pages 986 – 989, May 2000.

[48] S. Heier. *Grid Integration of Wind Energy Conversion Systems*. John Wiley & Sons, Ltd, Chicester, UK, 1998.

[49] S.A. Papathanassiou and M.P. Papadopoulos. Dynamic behavior of variable speed wind turbines under stochastic wind. *IEEE Transactions on Energy Conversion*, 14(4):1617–1623, Dec. 1999.

[50] J.G. Slootweg, S.W.H. de Haan, H. Polinder, and W.L. Kling. General model for representing variable speed wind turbines in power system dynamics simulations. *IEEE Transactions on Power Systems*, 18(1):144 – 151, Feb 2003.

[51] Database of wind characteristics. [Online]. Available: http://www.winddata.com.

[52] R. Mukund. *Wind and solar power systems*. CRC Press, CRC Press LLC, 2000 N.W., Corporate Blvd., Boca Raton, Florida 33431., 1999.

[53] B. Lindgren. *A Power Converter for Photovoltaic Applications.* PhD thesis, Department of Electric Power Engineering, Chalmers University of Technology, Göteborg, Sweden, 2000.

[54] K.H. Hussein, I. Muta, T. Hoshino, and M. Osakada. Maximum photovoltaic power tracking: an algorithm for rapidly changing atmospheric conditions. In *Generation, Transmission and Distribution, IEE Proceedings*, volume 142, pages 59 – 64, Jan 1995.

[55] M.F Ishengoma and E.E Norum. Design and implementation of adigitally controlled stand-alone photovoltaic power supply. In *Nordic Workshop on Power and Industrial Electronics(Norpie 2002)*, Stockholm, Sweden, 12-14 Aug 2002.

HELSINKI UNIVERSITY OF TECHNOLOGY CONTROL ENGINEERING LABORATORY

Editor: H. Koivo

Report 134 Elmusrati, M. S., Koivo, H. N.
Radio Resource Scheduling in Wireless Communication Systems. January 2003.

Report 135 Blomqvist, E.
Security in Sensor Networks. February 2003.

Report 136 Zenger, K.
Modelling, Analysis and Controller Design of Time-Variable Flow Processes. March 2003.

Report 137 Hasu, V.
Adaptive Beamforming and Power Control in Wireless Communication Systems. August 2003.

Report 138 Haavisto, O., Hyötyniemi, H.
Simulation Tool of a Biped Walking Robot Model. March 2004.

Report 139 Halmevaara, K., Hyötyniemi, H.
Process Performance Optimization Using Iterative Regression Tuning. April 2004.

Report 140 Viitamäki, P.
Hybrid Modeling of Paper Machine Grade Changes. May 2004.

Report 141 Pöyhönen, S.
Support Vector Machine Based Classification in Condition Monitoring of Induction Motors. June 2004.

Report 142 Elmusrati, M. S.
Radio Resource Scheduling and Smart Antennas in Cellular CDMA Communication Systems. August 2004.

Report 143 Tenno, A.
Modelling and Evaluation of Valve-Regulated Lead-Acid Batteries. September 2004.

Report 144 Hyötyniemi, H.
Hebbian Neuron Grids: System Theoretic Approach. September 2004.

Report 145 Hyötyniemi, H. (ed.)
Complex Systems: Science at the Edge of Chaos - Collected papers of the Spring 2003 postgraduate seminar. October 2004.

Report 146 Paanasalo, J.
Modelling and Control of Printing Paper Surface Winding. June 2005.

Report 147 Mohamed, F.
Microgrid Modelling and Simulation. March 2006.

ISBN-13 978-951-22-8417-7

ISBN-10 951-22-8417-0

ISSN 0356-0872

Picaset Oy, Helsinki 2006